Fourier Analysis of Sinusoidally Driven Thalamocortical Relay Neurons and a Minimal Integrate-and-Fire-or-Burst Model

GREGORY D. SMITH,[1,4] CHARLES L. COX,[3] S. MURRAY SHERMAN,[3] AND JOHN RINZEL[1,2,4]

[1]Center for Neural Science and [2]Courant Institute of Mathematical Sciences, New York University, New York, New York 10003; [3]Department of Neurobiology, State University of New York, Stony Brook, New York 11794; and [4]Mathematical Research Branch, National Institute of Diabetes and Digestive and Kidney Diseases, National Institutes of Health, Bethesda, Maryland 20814

Smith, Gregory D., Charles L. Cox, S. Murray Sherman, and John Rinzel. Fourier analysis of sinusoidally driven thalamocortical relay neurons and a minimal integrate-and-fire-or-burst model. *J. Neurophysiol.* 83: 588–610, 2000. We performed intracellular recordings of relay neurons from the lateral geniculate nucleus of a cat thalamic slice preparation. We measured responses during both tonic and burst firing modes to sinusoidal current injection and performed Fourier analysis on these responses. For comparison, we constructed a minimal "integrate-and-fire-or-burst" (IFB) neuron model that reproduces salient features of the relay cell responses. The IFB model is constrained to quantitatively fit our Fourier analysis of experimental relay neuron responses, including: the temporal tuning of the response in both tonic and burst modes, including a finding of low-pass and sometimes broadband behavior of tonic firing and band-pass characteristics during bursting, and the generally greater linearity of tonic compared with burst responses at low frequencies. In tonic mode, both experimental and theoretical responses display a frequency-dependent transition from massively superharmonic spiking to phase-locked superharmonic spiking near 3 Hz, followed by phase-locked subharmonic spiking at higher frequencies. Subharmonic and superharmonic burst responses also were observed experimentally. Characterizing the response properties of the "tuned" IFB model leads to insights regarding the observed stimulus dependence of burst versus tonic response mode in relay neurons. Furthermore the simplicity of the IFB model makes it a candidate for large scale network simulations of thalamic functioning.

INTRODUCTION

Considerable attention has been focused in recent years on the functioning of thalamic relays, because it has become clear that the thalamus does not serve as a simple, machine-like relay of information to cortex (for recent reviews, see Sherman and Guillery 1996, 1998). Instead the thalamus controls the extent and nature of information being relayed in a dynamic fashion that appears to be related to behavioral state and perhaps attentional demands. A good example is the lateral geniculate nucleus, the thalamic relay of retinal information to visual cortex. Only 5–10% of synapses on geniculate relay cells derive from retina. The rest derive from nonretinal sources, including local GABAergic cells, feedback afferents from visual cortex, and various pathways from the brain stem, and these modulate the nature of retinogeniculate transmission (Sherman and Guillery 1996, 1998).

In addition to the complexity of thalamic circuitry, the membrane properties of relay cells contribute to the nature of the relayed information. In particular, thalamic relay cells exhibit a voltage- and time-dependent, low-threshold, transient Ca^{2+} conductance, that, when activated, allows Ca^{2+} to enter the cell via T-type (for "transient") Ca^{2+} channels, producing a transmembrane current, I_T, and leading to a large depolarization known as the low-threshold Ca^{2+} spike. The inactivation state of I_T determines whether information is relayed to cortex in *tonic mode* or *burst mode* (Jahnsen and Llinas 1984a,b; Sherman 1996). When the cell starts off relatively depolarized (above roughly −60 mV for >50–100 ms), I_T is inactivated, and the relay cell responds to an excitatory input [e.g., a retinal excitatory postsynaptic potential (EPSP)] with sustained firing of unitary action potentials. This is the tonic firing mode. However, if the cell is hyperpolarized first (below roughly −65 mV for >50–100 ms), the inactivation of I_T is removed (i.e., I_T becomes deinactivated), and now a sufficient depolarization or EPSP will activate I_T. The result is a low-threshold Ca^{2+} spike with a brief burst of 2–10 action potentials riding its crest.

One of the keys to understanding how thalamic relays work is to understand in more detail how the input/output properties of relay cells are affected by the inactivation state of I_T. We sought to do this with both an experimental and modeling approach. By recording from relay cells of the lateral geniculate nucleus of the cat in vitro, we measured input/output properties by injecting into the cell sinusoidal currents that varied in amplitude, frequency, and mean level, and we performed analogous input/output experiments on a minimal relay cell model to test the degree to which the essential features of I_T accounted for relay cell responses. In addition to providing an easily parameterized set of stimuli that lends itself to Fourier analysis, the use of sinusoidal current injection allows us to interpret our results in the context of the spatial and temporal frequency analysis paradigm that has such a successful history in visual systems neuroscience (for review, see Shapley and Lennie 1985). Of course, our use of Fourier techniques is not based on an assumption of the linearity of relay neuron responses but simply reflects an historically preferred method of extracting relevant measures of cellular response (see METHODS).

For the theoretical component of this study, we developed a minimal "integrate-and-fire-or-burst" (IFB) neuron model. This model is constructed by adding a slow variable representing the deinactivation level of I_T to a classical integrate-and-

fire neuron model (Knight 1972). The IFB model is designed specifically to be as simple as possible while still quantitatively reproducing much of the empirically observed properties of the relay cells. One motivation for developing such a minimal model is to simplify the parameter selection process. Furthermore, because the IFB model is minimal, a detailed characterization of its response properties leads to insight regarding the stimulus dependence of burst versus tonic response modes in thalamic relay cells. A final motivation for development of the IFB model is to have a realistically tuned yet computationally undemanding relay cell model that can be used in large scale network simulations of thalamic function.

METHODS

Experimental methods

We performed intracellular recordings with the whole cell configuration on thalamic relay cells of young cats (5–8 wk of age) in compliance with approved animal protocols. We used a thalamic brain-slice preparation containing the lateral geniculate nucleus. Briefly, the animals were anesthetized deeply with 25 mg/kg ketamine and 1 mg/kg xylazine and a block of tissue containing the thalamic region was removed and placed in cold, oxygenated slicing solution containing (in mM) 2.5 KCl, 1.25 NaH_2PO_4, 10.0 $MgCl_2$, 0.5 $CaCl_2$, 26.0 $NaHCO_3$, 11.0 glucose, and 234.0 sucrose. Thalamic slices (250–300 μm) were cut in a coronal or sagittal plane with a vibrating tissue slicer and placed in a holding chamber (30°C) for >2 h before recording. Individual slices were transferred to a submersion-type recording chamber maintained at 30°C and continuously perfused with oxygenated physiological solution containing (in mM) 126.0 NaCl, 2.5 KCl, 1.25 NaH_2PO_4, 2.0 $MgCl_2$, 2.0 $CaCl_2$, 26.0 $NaHCO_3$, and 10.0 glucose, all at pH 7.4.

We used an Axoclamp 2A amplifier to obtain current-clamp recordings from geniculate relay neurons in the A-laminae, and we continuously monitored the bridge balance throughout the recordings. The recording pipette solution contained (in mM) 117.0 K-gluconate, 13.0 KCl, 1.0 $MgCl_2$, 0.07 $CaCl_2$, 0.1 EGTA, 10.0 HEPES, and 0.5% biocytin. Data were digitized, stored on-line using Axotape software (Axon Instruments), and also recorded onto VHS tape for off-line analysis. Current injection through the recording electrode consisted of a sinusoidal waveform with an AC component (I_1) that varied in both amplitude (50–800 pA) and frequency (0.1–100 Hz). The DC component (I_0) of the current waveform was altered to manipulate the firing mode of the neuron (i.e., burst vs. tonic). All experimental records of membrane potential of relay neuron in whole cell mode have been adjusted to account for a 10-mV junction potential.

Fourier analysis of experimental and theoretical responses

Customized user M-files were written for MATLAB 5.2.0 (The MathWorks) to perform data analysis using an SGI Challenge supercomputer that runs the IRIX operating system. For each stimulus condition, a periodic histogram (q_k, k an integer, $0 < k < N - 1$, $n = 64$ bins) was constructed that tallied over c cycles of period T the number of action potentials (q_k) evoked by the experimental or model relay neuron at each of N blocks of phase relative to the applied current's period. Accounting for the number of cycles recorded and the time represented by one bin of phase (i.e., for 64 bins, 1 bin is $\pi/32$ rad), we generated the (periodic) poststimulus response histogram (PSTH) defined by $Q_k \equiv q_k N/cT$. A discrete Fourier transform of this PSTH was performed, leading to a set of N complex valued numbers, $\hat{Q}_n$, given by (Press et al. 1992)

$$\hat{Q}_n = \sum_{k=0}^{N-1} Q_k \exp(-2\pi i k n/N) \tag{1}$$

each with an associated amplitude, $A_n = |\hat{Q}_n|$, and phase, $P_n = \arg(\hat{Q}_n)/2\pi$. With the preceding definitions, $F_0 = A_0/N$ has units of spikes/second and is the mean firing rate of the neuron; that is, $F_0 = q_{tot}/cT$, where $q_{tot} \equiv \Sigma_k q_k$ is the total number of spikes during the trial. The fundamental or stimulus-driven component of the response, F_1, is given by $F_1 = (A_1 + A_{N-1})/n = 2A_1/N$. (For the 2nd equality, we have used $A_1 = A_{N-1}$, which follows because the raw histogram, q_k, is real valued). As defined in the preceding text, P_1 is the phase advance or lag of this stimulus-driven response, has units of cycles, and takes values between -0.5 and $+0.5$. In addition, we define the following "index of nonlinearity"

$$\Gamma = \left[\sum_{n=1}^{N-1} (A_n)^2 - 2(A_1)^2 \right] \bigg/ \sum_{n=1}^{N-1} (A_n)^2 \tag{2}$$

This index of nonlinearity, Γ, is the normalized power of all modulated (non-DC) components of the PSTH not accounted for by the fundamental component of the response. Thus Γ takes values between zero (completely linear) and one (completely nonlinear). F_0, F_1, P_1, and Γ are the response measures of relay cells on which we shall concentrate.

For clarity of figure presentation, we also normalized the raw histogram, q_k, by the total number of spikes during the trial (q_{tot}). The result is a *spike phase density histogram* (SPDH), defined by $\rho_k \equiv q_k/q_{tot}$. This SPDH has unit area and represents the likelihood of observing an action potential at a particular phase of the applied current.

IFB model

GENERAL FEATURES. The IFB model is constructed by adding a slow variable to a classical integrate-and-fire model neuron. The slow variable, h, represents the inactivation of the low-threshold Ca^{2+} conductance, which involves T-type Ca^{2+} channels and produces a transmembrane current, I_T. The model equations are (Rinzel 1980)

$$C \frac{dV}{dt} = I_{app} - I_L - I_T \tag{3}$$

$$\frac{dh}{dt} = \begin{cases} -h/\tau_h^- & (V > V_h) \\ (1 - h)/\tau_h^+ & (V < V_h) \end{cases} \tag{4}$$

The current balance equation, *Eq. 3*, includes the sinusoidal applied current, $I_{app} = I_0 + I_1 \cos(2\pi f t)$; a constant conductance leakage current (I_L) of the form, $I_L = g_L(V - V_L)$; and the low-threshold Ca^{2+} current, I_T. An action potential occurs whenever the membrane potential reaches the suitable firing threshold (V_θ) such that $V(t) = V_\theta \Rightarrow V(t^+) = V_{reset}$.

Equation 4 is an idealization of the dynamics of I_T. The deinactivation level of I_T, h, relaxes to zero with time constant τ_h^- (=20 ms) when $V > V_h$ and relaxes to unity with time constant of τ_h^+ (=100 ms) when $V < V_h$. Sufficient hyperpolarization thus leads to increasing values of h, which represents deinactivation of I_T. For simplicity, we choose the following form for I_T

$$I_T = g_T m_\infty h(V - V_T) \tag{5}$$

where m_∞ is a characterization of the activation of I_T, $m_\infty = H(V - V_h)$, and $H(\cdot)$ is the Heaviside step function. In this form, the IFB model is capable of postinhibitory rebound bursting. The parameter τ_h^+ sets the duration of the burst, whereas the parameter τ_h^- sets the duration of hyperpolarization necessary to recruit a maximal postinhibitory rebound response.

In this form, the model is very simple—most of its behavior can be understood in terms of the dual thresholds, V_h and V_θ, that are responsible for the activation of burst and tonic spiking, respectively. Because a moderate range of applied currents was used experimentally, we found that it was not necessary to include an absolute

refractory period in the spike generation mechanism. That is, in the experimental results presented here, the saturating regime of a relay neuron's current-frequency relation rarely was sampled. Also for the sake of simplicity, we have not included in the model the hyperpolarization-activated cation conductance, I_h (also known as the "sag" current or I_{sag}).

We integrated *Eqs. 3* and *4* using a 266 MHz LINUX workstation running XPP, an ordinary differential equation solver written by Bard Ermentrout at the University of Pittsburgh and available via the internet (http://www1.pitt.edu/~phase/). All calculations were performed using the fourth-order Runge-Kutta integration method and a time step of 10–100 μs.

PARAMETER SELECTION.   Standard parameters were selected for the IFB model in the following fashion. First, experimental observations indicated that the resting membrane potential of the relay neurons recorded in vitro was -75 to -65 mV. In the absence of applied current (I_{app}), the leakage term (I_L) exclusively sets the resting potential of the neuron model. We thus set V_L to -65 mV. A second experimental observation is that the relay neurons recorded in vitro are hyperpolarized sufficiently at rest so that I_T is deinactivated. Indeed, quiescent relay neurons in the slice responded to a brief depolarization with a burst of action potentials. For this reason, we set V_h to -60 mV, ensuring that the threshold for activation (and deinactivation) of I_T is several millivolts greater than V_L, as observed experimentally. This value for V_h also roughly corresponds to the observed threshold for activation of bursts.

Although relay neurons from which we recorded were not physiologically identified as X or Y, we chose both the surface area ($S_A = 30,000 \ \mu m^2$) and capacitance ($C = 2 \ \mu F/cm^2$) of relay neurons to be in agreement with measurements performed on physiologically identified relay cells in the cat's lateral geniculate nucleus (Bloomfield et al. 1987). This value for S_A implies that a DC applied current of 300 pA corresponds to $I_{app} = I_0 = 1 \ \mu A/cm^2$ in *Eq. 3*. However, reported values of S_A are distributed over a range of 20,000–46,000 μm^2 for X relay cells and 33,000–55,000 μm^2 for Y relay cells (Bloomfield et al. 1987), and this could lead to a significant change in this correspondence.

With values for S_A and C fixed, the magnitude of the leakage conductance was chosen ($g_L = 0.035 \ mS/cm^2$) so that the rheobase of the IFB model fell within the experimentally observed range of 250–400 pA. This value of g_L corresponds to an input resistance of 95 MΩ, which also lies within the experimentally observed range. Next, $V_\theta = -35$ mV and $V_{reset} = -50$ mV were chosen so that the value for V_θ corresponded roughly to the observed tonic spiking threshold and the slope of the IFB model current-frequency relationship in tonic mode agreed with that of representative relay neurons. The time constants for deinactivation ($\tau_h^+ = 100$ ms) and inactivation ($\tau_h^- = 20$ ms) are taken from the experimental and theoretical literature (Coulter et al.1989; Huguenard and McCormick 1992; Wang et al. 1995). Finally, the maximum conductance associated with I_T ($g_T = 0.07 \ mS/cm^2$) was chosen so that the IFB model reproduces the experimentally observed maximum of ~5–10 spikes/burst for relay neurons in the slice preparation.

RESULTS

Current-clamp recordings from a total of 12 relay neurons from the lateral geniculate nucleus of the cat were included in the present study. All cells displayed physiological characteristics consistent with healthy relay neurons, including a hyperpolarization-activated sag current (I_h), burst discharge, and overshooting action potentials. Cells included in this study had an average resting membrane resting potential of -67.8 ± 4.1 mV (mean $\pm$ SD) and an input resistance that averaged 153.0 ± 38.0 MΩ.

The preferred firing mode of the relay cell—tonic or burst—was controlled largely by constant current injection from the recording pipette. This constant current injection is referred to in the following text as I_0, which we varied between experiments from -400 to 800 pA. On top of this constant current, we injected various other currents, usually sinusoidal at various frequencies and amplitudes. At relatively depolarized membrane potentials (i.e., more positive values of I_0), the cell fired to the sinusoidal current in tonic mode, whereas at relatively hyperpolarized membrane potentials (i.e., more negative values of I_0), the cell fired in burst mode; at intermediate levels of membrane potential, responses often consisted of a burst followed by tonic firing. It is noteworthy that in all cases when we saw both response modes to a cycle of the current injection, burst firing always preceded tonic firing.

General responses to current injection

In Fig. 1*A,* the results of current steps injected into the relay cell experimentally are shown. When the membrane potential (V_m) was adjusted initially to -58 mV (V_{hold}; $I_0 = 230$ pA), the neuron discharged in tonic mode in response to a short current pulse (200 pA). However, at a more hyperpolarized V_{hold} (-77 mV), a depolarizing current step (50 pA) evoked a transient burst of high-frequency action potentials. The IFB model produces both tonic and burst responses (Fig. 1*B*) that are similar to those produced experimentally. Figure 1*B* also shows the inactivation gating variable of the simulated low-threshold Ca^{2+} current (denoted by h; see METHODS) dropping from unity to near zero shortly after the onset of the current pulse. In the IFB model, the time scale of this inactivation determines the length of the burst event. The value of h remains near zero (representing inactivation of the low-threshold Ca^{2+} conductance) until the depolarizing pulse ends, at which point the membrane potential drops below V_h, the threshold for deinactivation of I_T, and h recovers toward 1.

Figure 2*A* presents experimental recordings that illustrate firing patterns of a geniculate relay neuron during sinusoidal current injection over a range of stimulation amplitudes (I_1) while the modulation frequency is held constant at 1 Hz. In Fig. 2*A, left,* the neuron is in tonic mode, because of a more depolarized I_0 of 335 to 498 pA, whereas in the *right column,* the cell is hyperpolarized because of a more hyperpolarized I_0 of -4 to -136 pA and responds with burst discharges. When the neuron responds in tonic mode, the average number of spikes/cycle increases as I_1 is increased. In contrast, in burst mode, the neuron responds with 1 burst/cycle over a wide range of I_1, and the number of spikes/burst remains relatively constant at 7 or 8. An exception to this occurs at the lowest-modulation amplitudes, where the neuron bursts once for every several cycles of applied current (Fig. 2*A, top right*). In this paper, we will refer to such behavior as a *subharmonic* burst response. In addition to these representative patterns of cell responses to 1 Hz stimulation, we also observed *super*harmonic burst responses (2 bursts/cycle), subharmonic tonic responses, and burst followed by tonic responses.

Figure 2*B* presents a series of IFB model calculations for comparison with Fig. 2*A*. These calculations were performed using identical cellular parameters (see Table 1), whereas applied current parameters were chosen in qualitative agreement with the experimental conditions used in Fig. 2*A*. The
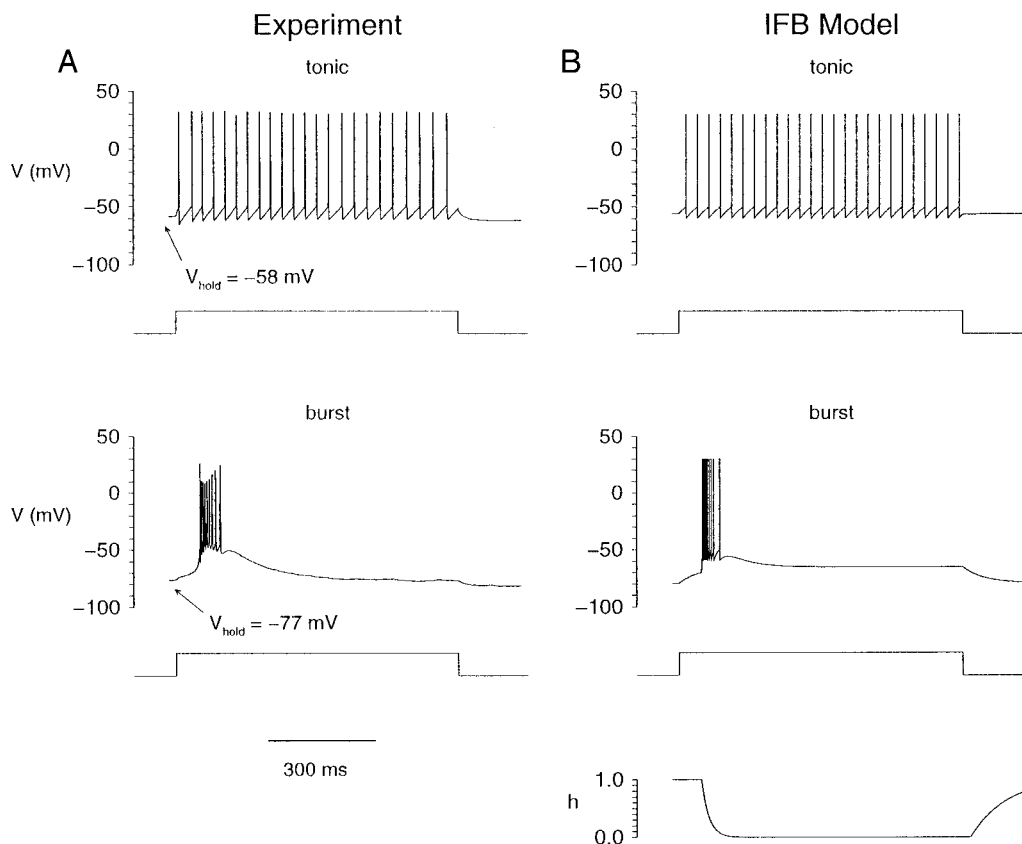
FIG. 1. Experimental records of relay neuron responses to depolarizing current steps and comparable integrate-and-fire-or-burst (IFB) model simulations. *A*: relay neuron responds in either tonic or burst mode depending on the initial membrane potential (V_{hold}). For tonic (or burst) responses, V_{hold} in mV, initial applied current and applied current level during pulse in pA: -58, 230, and 430 (or -77, -350, -300). *B*: IFB model reproduces both tonic and burst responses depending on the initial membrane potential. Applied current initially and during pulse in $\mu A/cm^2$: 0.67, 1.33 (-0.16, 0.34). *Bottom*: *h*, the deinactivation gating variable for I_T, during the IFB model burst response. Cellular parameters: $g_T = 0.8$ mS/cm^2; in mV: $V_\theta = -50$, $V_{reset} = -60$, $V_h = -70$, and $V_L = -75$. Other parameters as in Table 1.

simulations reproduce many salient features of the experimental recordings. For example, the IFB model responds in tonic mode to more depolarizing mean applied current (I_0) and in burst mode to more hyperpolarizing I_0. In tonic mode, the average number of spikes/cycle increases as a function of I_1, whereas in burst mode, 1 burst/cycle is observed over a wide range of I_1. In addition, the IFB model produces 7–8 spikes/burst, relatively independent of I_1. Although the IFB model reproduces the overall pattern of responses to a range of stimulus conditions in both tonic and burst responses, it does not reproduce the subharmonic responses observed at low modulation amplitude (cf. Fig. 2, *A* and *B, top right*; see DISCUSSION).

Figure 3*A* consists of recordings from the same neuron as Fig. 2*A*, but here sinusoidal current injection over a range of I_0 values and stimulation frequencies is applied while I_1 is fixed. When the holding V_m is adjusted so that the neuron is in a tonic firing mode (depolarized I_0; *left*), the cell exhibits tonic firing in response to I_1 frequencies of 0.3, 1, and 3 Hz, and is unresponsive to 10 Hz. The average number of spikes/cycle decreases in tonic mode as frequency is increased. However, when the neuron is in burst mode (hyperpolarized I_0; *right*), 1 burst/cycle (5–8 spikes/burst) is observed in response to 0.3 and 1 Hz until subharmonic responses are evoked at 3 Hz; no response was seen at 10 Hz. The subharmonic responses were

observed most commonly in response to a frequency of 3 Hz, occasionally at 1 Hz. Many other cells did respond to 10 Hz stimulation, especially in tonic mode (see following text). In 4 of 12 cells, superharmonic responses of 2 bursts/cycle were observed at low stimulation frequencies (0.1–0.3 Hz; see following text).

Figure 3*B* presents a series of IFB model calculations that reproduce many salient features of the experimental results shown in Fig. 3*A*. For example, when the model responds in tonic mode (*left*), the average number of spikes per cycle decreases as frequency increases. Yet when the model responds in burst mode, 1 burst/cycle is observed over a wide range of frequencies of I_1. At the cutoff frequency of 10 Hz, both the relay neuron and the IFB model are unresponsive, and the effect of the mean applied current, I_0, on the mean membrane potential can be seen clearly (see Fig. 3, *bottom*). The IFB model thus qualitatively reproduces the neuron responses over a range of stimulus frequencies with the exception of subharmonic responses.

Superharmonic burst responses

As mentioned in the preceding text, burst responses observed at low frequency were primarily 1 burst/cycle (1:1). However, superharmonic burst responses were sometimes ob-
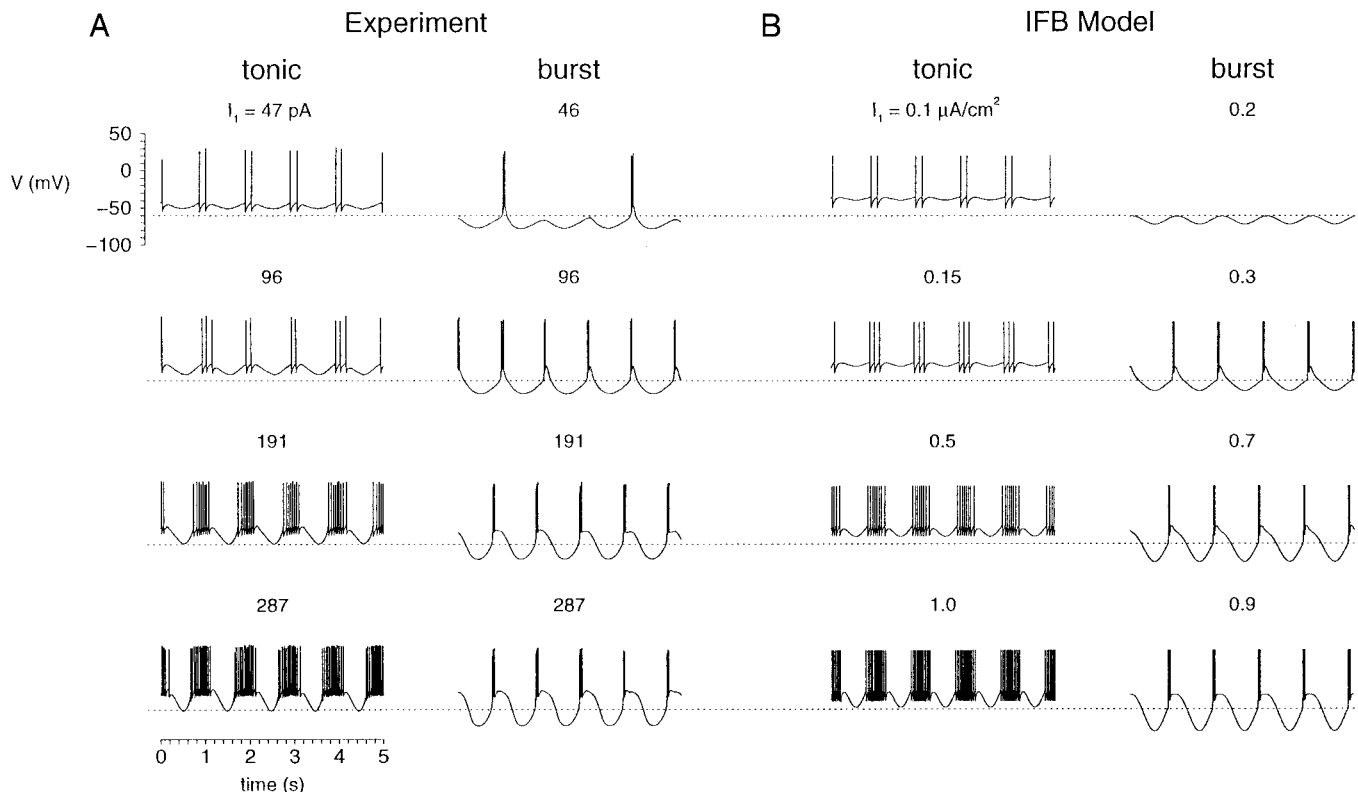
FIG. 2. *A*: whole cell recordings of a single relay neuron showing representative firing patterns during 1-Hz sinusoidal current injection over a range of modulation amplitudes (I_1). Tonic or burst responses are evoked depending on the value of the mean applied current (I_0), which is 335–498 pA for tonic firing and −4 to −136 pA for burst firing. During tonic responses, the average number of spikes/cycle increases as I_1 is increased in successive rows. Subharmonic burst responses are observed for low I_1, but otherwise 1 burst/cycle is observed. *B*: behavior of the IFB model. When stimulus parameters are varied in qualitative agreement with *A*, the IFB model reproduces many salient features these responses. With depolarizing mean applied current ($1.0 \, \mu A/cm^2 < I_0 < 1.2 \, \mu A/cm^2$), the IFB model responds in tonic mode and the average number of spikes/cycle increases as I_1 is increased in successive rows. With hyperpolarizing mean applied current ($I_0 = -0.05 \, \mu A/cm^2$), the IFB model responds in burst mode. One burst/cycle is observed over a wide range of I_1. In this figure and all that follow, cellular parameters are as in Table 1 unless otherwise noted.

served at low frequencies. Examples recorded from two geniculate relay cells of single (1:1) and double (2:1) burst responses at low frequency are shown in Fig. 4, *A* and *B*, respectively. Figure 4, *left,* shows responses to a more hyperpolarized I_0, and the *right* shows responses to a more depolarized I_0 (see legend for details). The result is pure burst responses on the left and burst followed by tonic responses on the right. Because super-

TABLE 1. *Standard parameters for the IFB model*

Parameter	Value	Unit
Cellular parameters		
V_θ	−35	mV
V_L	−65	mV
C	2	$\mu F/cm^2$
g_L	0.035	mS/cm^2
V_{reset}	−50	mV
V_h	−60	mV
V_T	120	mV
τ_h^-	20	ms
τ_h^+	100	ms
g_T	0.07	mS/cm^2
Stimulus parameters		
I_0	−0.67–2.67	$\mu A/cm^2$
I_1	0–1.33	$\mu A/cm^2$
f	0.1–100	Hz

IFB, integrate and fire or burst.

harmonic burst responses were seen in response to the lowest temporal frequencies tested, which was 0.1 Hz, the prevalence of these two response types in our data have been quantified in the following way. There were a total of 56 trials collected from 12 different cells that exhibited bursts at 1–3 Hz. Of these, we quantified the response type at the lowest frequency tested, 0.1 Hz. The majority (61%) were 1:1 (i.e., 1 burst/cycle as in Fig. 4*A*). Superharmonic bursts (i.e., 2:1 as in Fig. 4*B*) were observed in 14% of the trials, whereas 3 bursts/cycle (3:1) were never observed. Interestingly, in the remaining 25% of trials, no response at all was observed at 0.1 Hz. However, at a higher frequency (0.3 Hz), only 3 of 56 trials (5%) exhibited no response, indicating that burst mode for some neurons has a genuine band-pass character to varying temporal frequency (see following text).

Responses as a function of frequency and amplitude of current injection

The filtering characteristics of relay neurons differ depending on the firing mode of the neuron. Figure 5 summarizes responses of two relay cells in both burst (hyperpolarized I_0) and tonic mode (depolarized I_0) to different levels of I_1 and frequency of current injection. The responses have been categorized into the following four classes: burst followed by tonic
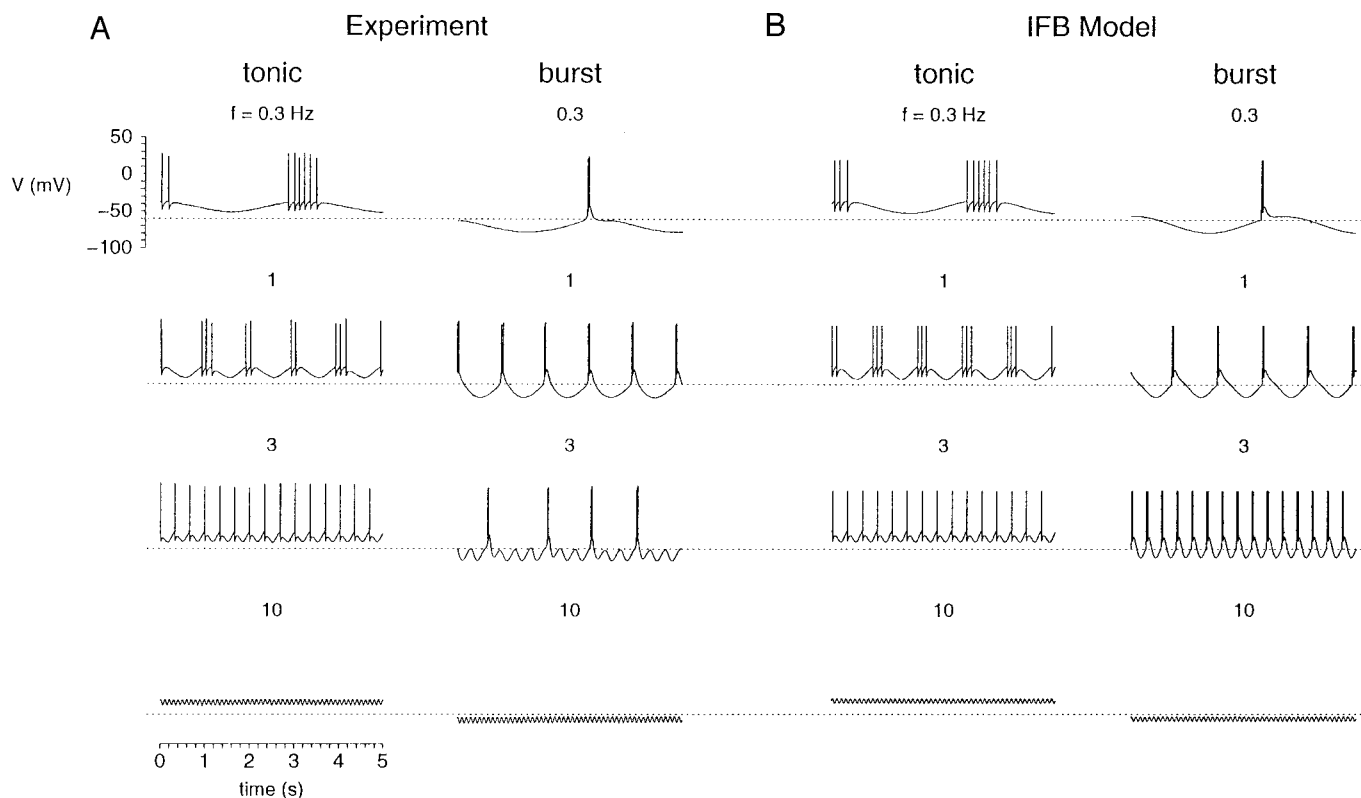
FIG. 3. *A*: intracellular recordings from the same neuron as Fig. 2*A* showing responses to sinusoidal current injection over a range of frequencies (f) while the modulation amplitude is held constant ($I_1 = 96$ pA). Relay neuron responds in tonic mode when a depolarizing mean applied current ($I_0 = 336$ pA) is applied and responds in burst mode when I_0 is hyperpolarizing ($I_0 = -136$ pA). One burst/cycle is observed over a range of frequencies and subharmonic responses are observed as the cutoff frequency of 3 Hz is approached. *B*: IFB model responses that reproduce these firing patterns. IFB model responds in tonic mode when the mean applied current is depolarizing ($I_0 = 0.8$ μA/cm^2). Average number of spikes/cycle decreases as f is increased in successive rows; at 10 Hz, the model no longer responds with tonic spikes. IFB model responds in burst mode when the mean applied current is hyperpolarizing ($I_0 = -0.05$ μA/cm^2). One burst/cycle is observed over a wide range of f; bursts cease at $f = 10$ Hz. $I_1 = 0.2$ μA/cm^2.

(filled circles), only burst (open circles, *left*) or only tonic (open circles, *right*), subharmonic burst (asterisks, *left*) or subharmonic tonic response (asterisks, *right*), and no response (dashes). Figure 5*A, left,* summarizes the responses of one of these neurons in burst mode. At low I_1 (50 pA), this neuron responded to 3 Hz with subharmonic bursts (asterisks) and gave no responses to higher or lower frequencies. With increasing I_1 (100 pA), the cell now responds 1:1 at 0.3 and 1 Hz, subharmonic at 3 Hz, but is still unresponsive to 0.1 Hz. With further increases in I_1 (200 pA), the neuron now responds to the full range of 0.1–3 Hz, but is unresponsive to 10 Hz. Thus burst responses of this cell show band-pass filtering for lower I_1 and low-pass filtering for higher I_1—in the latter case, the high-frequency cutoff increases to 10 Hz for $I_1 = 300$pA. Similar results from a second neuron responding in burst mode are presented in the Fig. 5*B, left*.

In tonic mode (Fig. 5, *right*), similar values of I_1 and frequency produce a different pattern of responses than observed in burst mode. First, all responses in tonic mode exhibit either low-pass or broadband filtering; there is no band-pass filtering because the cells always respond well to the lowest frequencies tested. Second, the high-frequency cutoff was greater in tonic than in burst mode, and for high values of I_1, there may be no observable cutoff frequency (Fig. 5*A, top right*). In this example, no high-frequency cutoff is observed

because I_0 was greater than the rheobase of neuron, whereas in the other example (Fig. 5*B, right*), I_0 was less than the rheobase. It is also notable that subharmonics in tonic mode, when apparent, generally occurred before the cutoff frequency.

Fourier analysis of relay cell and IFB model responses

To compare quantitatively the different consequences of burst and tonic firing modes on relay cell responses to sinusoidal current injection, we performed Fourier analysis of the intracellular recordings (see METHODS). SPDHs were constructed from experimental recordings, and Fig. 6 shows examples of how this is done for several different stimulus conditions producing burst, tonic, or burst followed by tonic firing (see following text for details of stimulation parameters). Figure 6*A* shows responses to four cycles of the injected current. Figure 6*B* shows these responses aligned on a cycle-by-cycle basis, and Fig. 6*C* shows SPDHs constructed by assigning each spike to 1 of 64 bins depending on the value of its phase with respect to I_1. In the resulting histograms, the spike density, ρ, approximates the likelihood of a neuron firing an action potential at a given phase, ϕ, of I_{app}. To quantify the dependence of the SPDHs on stimulus parameters (f, I_0, and I_1), discrete Fourier transforms of such histograms were performed leading to the assignment of four response measures:
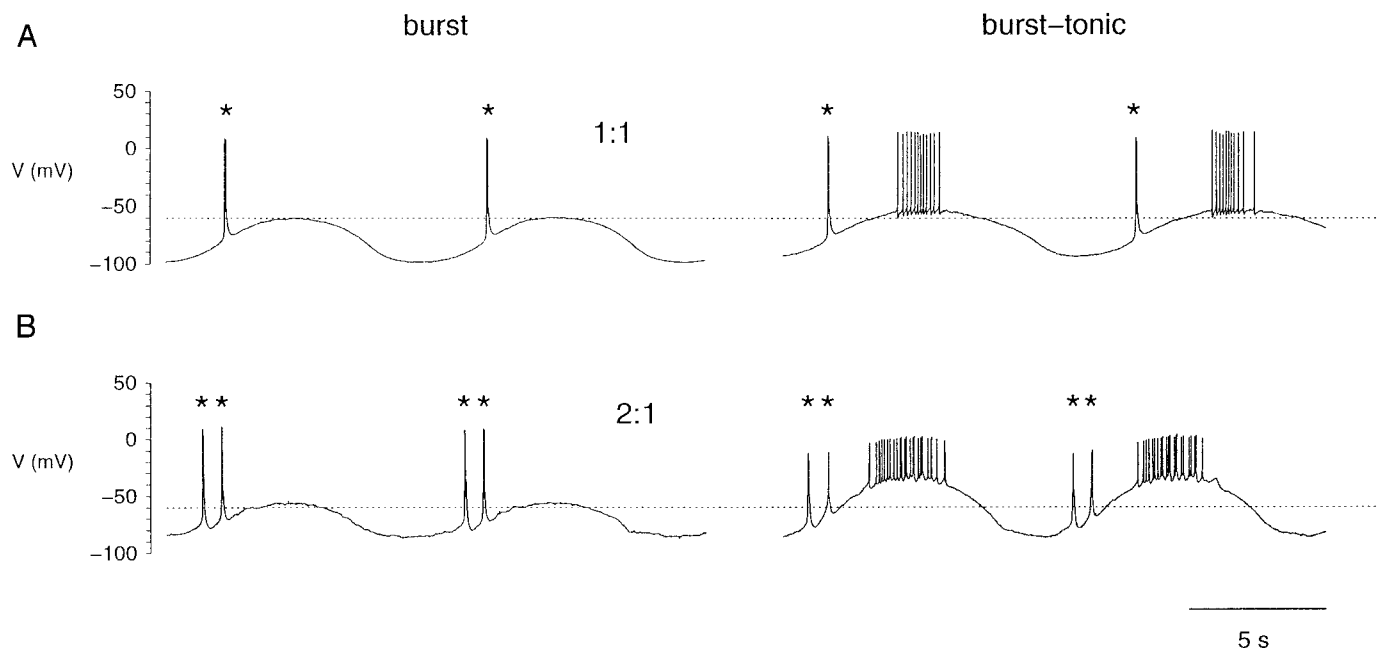
FIG. 4. Representative responses for relay neurons driven at low frequencies. Asterisks indicate bursts. *A*: at 0.1 Hz, this relay neuron responds with 1:1 bursting (i.e., 1 burst/cycle). *B*: different relay neuron responds to 0.1-Hz stimulation with 2:1 superharmonic bursting (i.e., 2 bursts/cycle). In both cases, increasing I_0, I_1, or both leads to the recruitment of tonic spikes and the generation of a burst followed by tonic (*burst-tonic*) response. I_0/I_1 in pA for the burst and the burst followed by tonic firing case, respectively: *A*, 0/300, 130/300; *B*, 60/150, 170/240.

F_0, the mean firing rate; F_1, the stimulus- or modulation-driven component of the response; P_1, the phase advance or lag of the modulation-driven response; and Γ, the nonlinearity of the response.

Figure 6*C* shows examples of SPDHs that are representative of our results from relay cells exhibiting tonic, burst, and burst followed by tonic responses obtained at 0.3 Hz. When stimulus parameters were such that the neuron responded in tonic mode ($I_0 = 410$ pA and $I_1 = 150$ pA), the SPDH approximates the shape of a rectified cosine. When stimulus parameters were such that the neuron responded in burst mode ($I_0 = -4$ pA and $I_1 = 50$ pA), the SPDH does not approximate a rectified cosine but rather shows a sharp peak near $\phi = -0.25$ (i.e., a 90° phase advance). These features are combined in a SPDH generated from intracellular records that exhibited burst followed by tonic responses (Fig. 6*C*). The burst and tonic portions of this response are separated by ~10°, and because the burst *always* proceeds the tonic response of each cycle, there is a gap in the SPDH.

INTERPRETATION OF RESPONSE MEASURES. Because many of the results to follow involve the relationship between the response measures, F_0, F_1, P_1, and Γ, it is instructive to review our expectations of these measures. Imagine an idealized tonic response of a neuron to be proportional to the rectified cosine (see Fig. 6*C*), most commonly

$$Q_{RC}(\phi) = \frac{1}{2} Q_{RC}^0 H(1 - 2R + \cos(2\pi\phi))[1 - 2R + \cos(2\pi\phi)]$$

$$(0 < R < 1) \quad (6)$$

where R indicates the degree of rectification, $H(\cdot)$ is the Heaviside step function, and the maximum response is given by

$$Q_{RC}^{max} = Q_{RC}^0(1 - R) \quad (7)$$

Figure 7*E* shows examples of SPDHs of this form and Fig. 7, *A* and *B*, shows the resulting dependence of the response measures F_0 and F_1 (open circles with solid line) on the degree of rectification, R. As expected, both F_0 and F_1 are decreasing functions of R, because rectification decreases both the mean firing rate and modulation-driven component of the rectified cosine response. Figure 7*C* shows for tonic firing the quotient F_1/F_0 as a function of R. This plot indicates that a sinusoidal response with no rectification (and a mean equal to its modulation amplitude) will have $F_1/F_0 = 1$. Conversely, highly rectified responses will have F_1 approximately twice as large as F_0.

For comparison, Fig. 7*F* shows PSTHs similar to those we observed from burst responses. These histograms are square pulses of the form

$$Q_{SP}(\phi) = \begin{cases} Q_{SP}^0 & \text{for } -(1-R)/2 < \phi < (1-R)/2 \\ 0 & \text{otherwise} \end{cases} \quad (8)$$

Figure 7, *A* and *B*, shows that the dependence of F_0 and F_1 on the degree of rectification, R, is different for square pulses and rectified cosines. For example, in the case of square pulse responses (open squares with solid line), F_0 decreases linearly and F_1 is nonmonotonic, reaching a maximum when the square pulse occupies one-half of the stimulus cycle.

Figure 7*D* shows the index of nonlinearity (Γ) expected for square pulse and rectified cosine responses, respectively. When a sinusoidal response shows no rectification ($R = 0$, *leftmost* open circle), the index of nonlinearity (Γ) is zero, because the power in F_0 and F_1 account for the entire histogram. Although an extremely high degree of rectification ($R = 1$) can lead to an index of nonlinearity near unity, the tonic responses we observed experimentally were always less than three-fourths rectified (cf. Fig. 7*E*). We thus expect, according to the plot of Γ
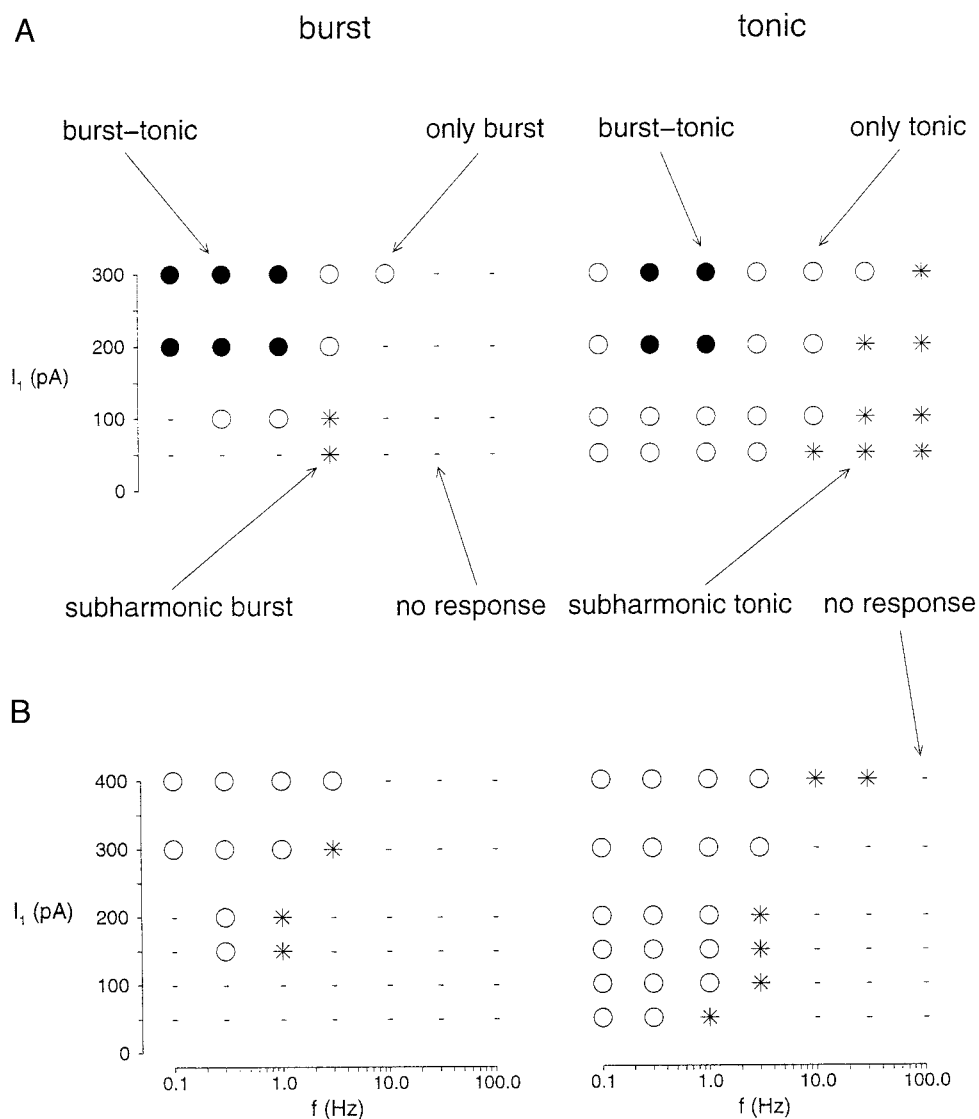
FIG. 5. For a range of applied current modulation amplitude (I_1) and frequency (f), the responses of 2 representative relay neurons, A and B, are categorized as burst followed by tonic firing (*burst-tonic*; filled circles), only burst or only tonic (open circles), subharmonic burst or subharmonic tonic (stars), and no response (dash). Superharmonic burst responses were not exhibited by either neuron. Burst followed by tonic responses also were observed at I_1 values of 600 pA (not shown).

in Fig. 7D, that low-frequency tonic responses will generally have an index of nonlinearity <0.3 (open circles with solid line). Similarly, Fig. 7D shows that the index of nonlinearity (Γ) of square pulse responses can be large or small depending on R (dotted and solid lines with open squares). However, because experimentally observed SPDHs generated from burst responses always had R values >0.85 (solid lines), the indices of nonlinearity observed were also high ($\Gamma > 0.7$). Thus during low-frequency stimulation, when relay cell responses resemble the histograms shown in Fig. 7, E and F, we expect the index of nonlinearity, Γ, to be highly correlated with the burstiness of the response.

FOURIER ANALYSIS OF EXPERIMENTAL DATA. With this background, Figs. 8 and 9 present the results of Fourier analysis of the responses of a population of relay cells showing burst and tonic responses to sinusoidal current injection. Only data involving pure burst or tonic responses (i.e., no burst followed by tonic responses) are shown here, which means that these data reflect mostly small values of I_1 and/or extremely hyperpolarized or depolarized values of I_0. Figure 8, A–D, summarizes experimental results from 84 trials (8 different cells) in which only burst responses were observed. When plotted in units of

spikes/second, the mean firing rate (F_0) is approximately half the value of the modulated response (F_1), and both are bandpass with peaks at 3 Hz (Fig. 8A). These data subsequently are plotted in units of spikes/cycle (Fig. 8B), showing that, at lower frequencies, a relatively constant number of spikes/cycle are observed, and in the majority of cases, these result from one burst/cycle.

Figure 8C shows the phase (P_1) of the F_1 response component as a function of frequency. At 3 Hz, the phase is nearly zero, meaning that the response is centered around the times that the applied current is maximum. At lower frequencies, the phase of the burst response advances toward one-quarter of a cycle at 0.1 Hz. This phase advance can be seen clearly in Fig. 8E, which shows SPDHs for a representative single neuron stimulated at four frequencies between 0.1 and 3 Hz. For example, the response at 0.1 Hz is centered near $\phi = -0.25$, whereas the response at 3 Hz is centered near $\phi = 0.10$.

Because the response in burst mode is focused at a particular phase at low frequencies, the index of nonlinearity (Γ) of burst responses is high for all injection frequencies that elicit a response (see Fig. 8D). At 3 Hz each of the 64 bins of phase represents ~5 ms, as opposed to 150 ms in the 0.1 Hz case); thus in Fig. 8E, the
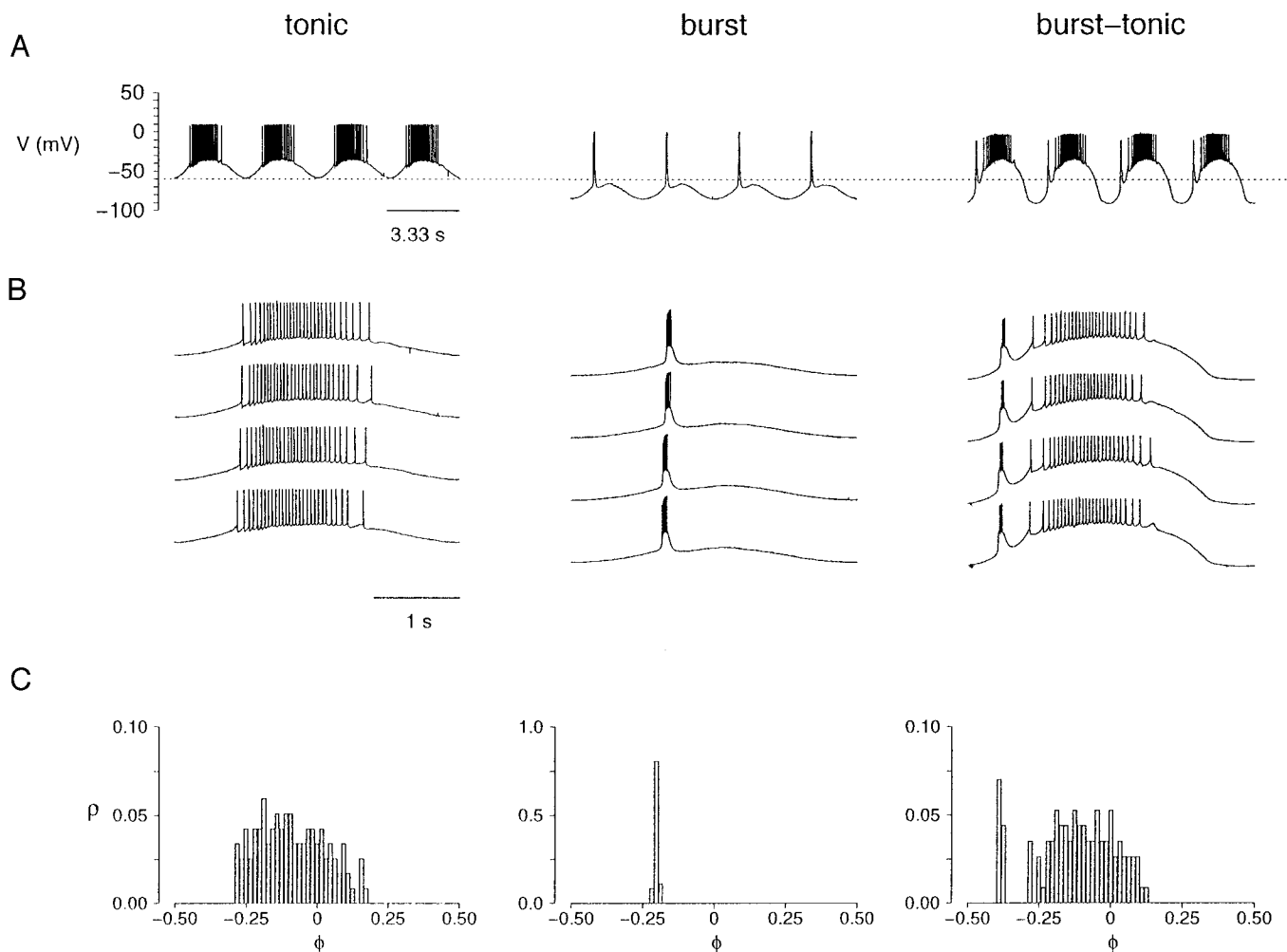
FIG. 6. Preliminary steps in the analysis of experimental data and simulation results. *A*: experimental voltage time courses (or simulation results) were obtained for several cycles of a stimulus with fixed parameters (f, I_0, and I_1). Here experimental voltage time courses that exhibit tonic, burst, and burst followed by tonic responses to stimulation at 0.3 Hz are presented. *B*: responses were aligned and each action potential was assigned a phase ($-0.5 < \phi < 0.5$) with respect to the sinusoidal applied current, phase zero being defined to occur when the applied current is maximum. *C*: spike phase density histogram (SPDH) was constructed by assigning each spike to 1 of 64 bins depending on the value of its phase. Resulting histogram represents the likelihood of a spike occurring at a given phase of the applied current. Discrete Fourier transforms were performed on these SPDHs leading to the calculation of the response measures, F_0, F_1, P_1 and Γ (see METHODS).

3-Hz burst response appears less focused. This spread of the burst response as a function of phase causes Γ to drop slightly at 3 Hz. Like most of the neurons from which we recorded, those illustrated in Fig. 8 did not respond at $\geq$10 Hz. However, this observed cutoff frequency does not necessarily correspond to the intrinsic upper limit for a relay cell in burst mode, because both experimentally (see Fig. 5*A*) and theoretically (see APPENDIX), the cutoff frequency is a function of the applied current parameters, I_0 and I_1. A small value of I_1, for example, often leads to a lower cutoff frequency (see Fig. 5).

Fourier analysis of relay cell responses to sinusoidal current injection in tonic discharge mode shows a pattern distinct from that observed for burst firing mode. Figure 9, *A–D*, summarizes experimental data from 88 trials (10 different cells) in which only tonic responses were observed. Similar to burst responses, during tonic firing, F_0 was generally less than F_1 (Fig. 9, *A* and *B*). The responses of these neurons in spikes/second do not show a high-frequency cutoff (Fig. 9*A*) because, for the majority of neurons included in this sample, I_0 is superthreshold

for firing action potentials (cf. Fig. 5*A*). Figure 9*B* shows that when these responses are replotted in spikes/cycle, the number of spikes/cycle increases at lower frequencies, a pattern distinct from burst mode (cf. Fig. 8*B*).

The phase of tonic responses shows a gradual reduction with increasing stimulation frequency, from ~0.1 cycles advanced at 0.1 Hz and to a similar amount delayed at 100 Hz. The index of nonlinearity (Γ) of tonic responses reaches a maximum of 0.8 at 3 Hz, which is, coincidentally, a value comparable to that of burst responses at the same frequency. This might seem at odds with the predictions summarized in Fig. 7*D*. However, this elevated Γ is due to phase locking to 3-Hz stimulation that is apparent in the SPDHs presented in Fig. 9*E*. In this phase-locked superharmonic response, each of 3–4 spikes/cycle produces an identifiable peak in the SPDH. As a result of this phase locking, the response profile is considerably distorted from a rectified cosine. The significance of such phase locking for functioning of relay cells is considered in the following text and in DISCUSSION.
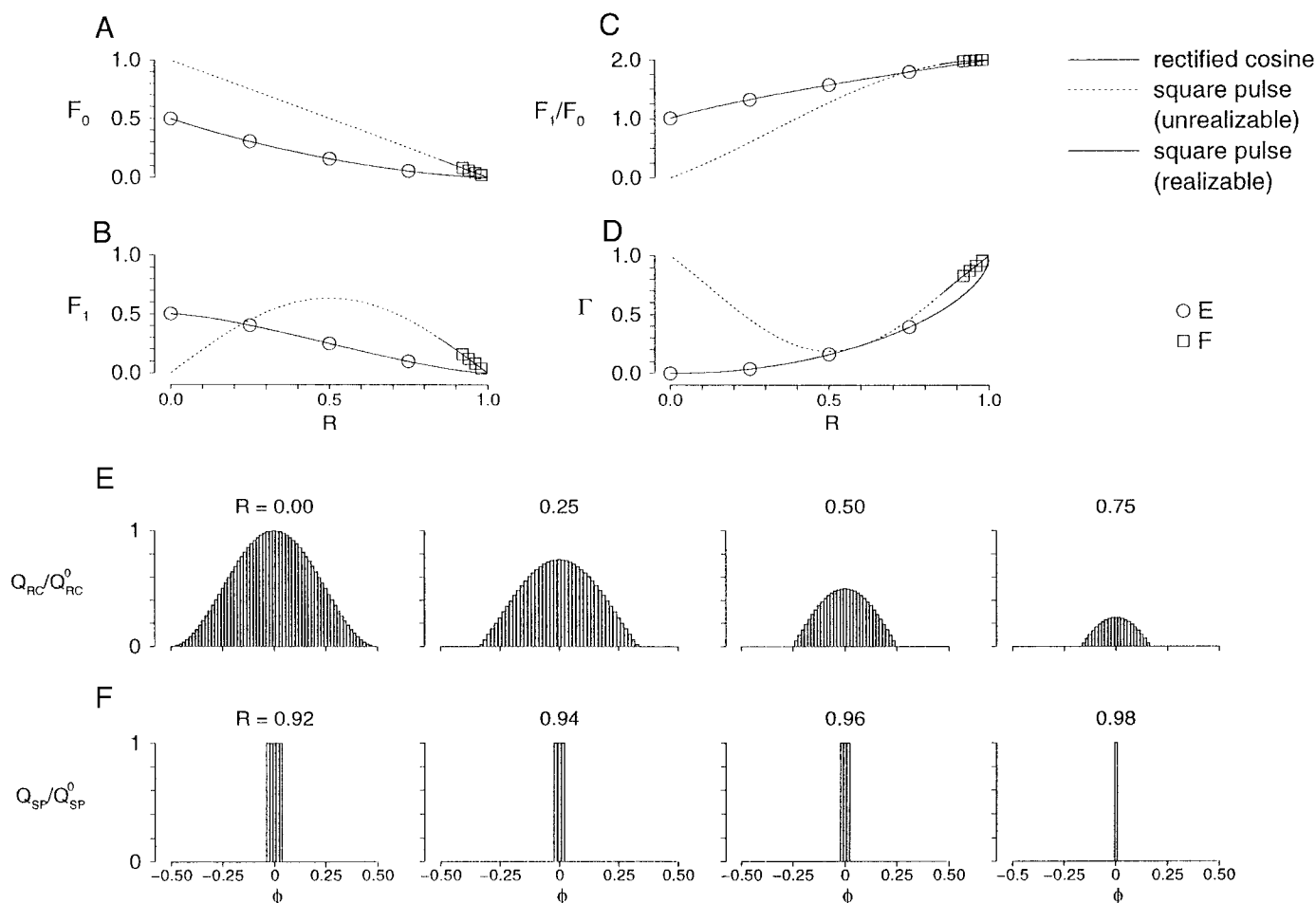
FIG. 7. Analytic calculation of response measures, F_0, F_1, and Γ, for rectified cosine and square pulse responses given by *Eqs. 6* and *8*, respectively. *A*: solid line with open circles shows the normalized fundamental response as a function of the degree of rectification (R) when the poststimulus response histograms (PSTHs) are rectified cosines (see *Eq. 6* and *E* for examples). Dotted line and solid line with open squares show the analogous calculation when the PSTHs are square pulses (see *Eq. 8* and *F*). Solid (*realizable*) portion of the plot indicates the range of R that is experimentally observed during burst responses; dotted (*unrealizable*) portion indicates the range not observed ($R < 0.85$), due to the fact that a maintained burst response requires the stimulus to be hyperpolarizing during a significant fraction of the stimulus cycle. *B–D*: calculations similar to *A* for the fundamental response (F_1), the ratio F_1/F_0, and the index of nonlinearity (Γ), each plotted as a function of R for both the square pulse and rectified cosine cases. *E* and *F*: PSTHs for square pulse and rectified cosine responses that correspond to open circles and squares in *A–D*.

The SPDHs of Fig. 9*E* show a gradual transition from superharmonic tonic responses to phase-locked subharmonic tonic responses that is ubiquitous in our recordings and indicated by notation of the form, *S:C*, on the histograms (*S* spikes for every *C* cycles). Superharmonic tonic responses (many spikes/cycle) are observed when the stimulating frequency is low (0.1–1 Hz). At a frequency of 3 Hz, phase-locked superharmonic spiking (3:1 to 4:1) begins, whereas at slightly higher frequencies (10 Hz), the neuron exhibits phase-locked action potentials exactly once per cycle (1:1). At higher frequencies of 30–100 Hz, the neuron responds with subharmonic tonic spikes (1:2 to 1:14) that are approximately phase locked to the applied current. Although the highest frequency at which 1:1 tonic spiking is observed is 10 Hz (see Fig. 9*E*), this does not reflect an intrinsic limit but rather depends on the particular values of I_0 and I_1 used (see DISCUSSION and APPENDIX).

Comparing the frequency-dependence of Γ in burst (Fig. 8*D*) and tonic (Fig. 9*D*) mode, we observe that at frequencies <1 Hz, Γ correlates with the burstiness of the response. However, at higher frequencies, the phase locking of tonic re-

sponses leads to elevated Γ that is distinct from nonlinearity arising from rectification (Fig. 7*D*). We also observe that at 0.1 Hz, Γ exceeds 0.16, the value expected for a half-wave rectified but otherwise linear response (as shown in Fig. 7*D*).

FOURIER ANALYSIS OF THE IFB MODEL. Figures 10 and 11 present the results of Fourier analysis applied to IFB model responses. As in Figs. 8 and 9, I_0 and I_1 are chosen to ensure pure tonic or burst responses from the model (burst followed by tonic responses are considered in the following text). For burst firing, there is a remarkable, quantitative equivalence between experiment (Fig. 8) and theory (Fig. 10). One subtle difference is that the IFB model phase locks more precisely than actual relay cells (cf. 3-Hz SPDHs in Figs. 8*E* and 10*E*). This may be due to the presence of noise in the voltage recordings that is absent in the IFB model. Indeed, when the simulated applied current is supplemented with Gaussian noise (mean amplitude of 0 pA and a variance similar to that of I_1), phase locking by the IFB model is strongly attenuated (data not illustrated), and the nonlinearity index (Γ) is reduced. IFB
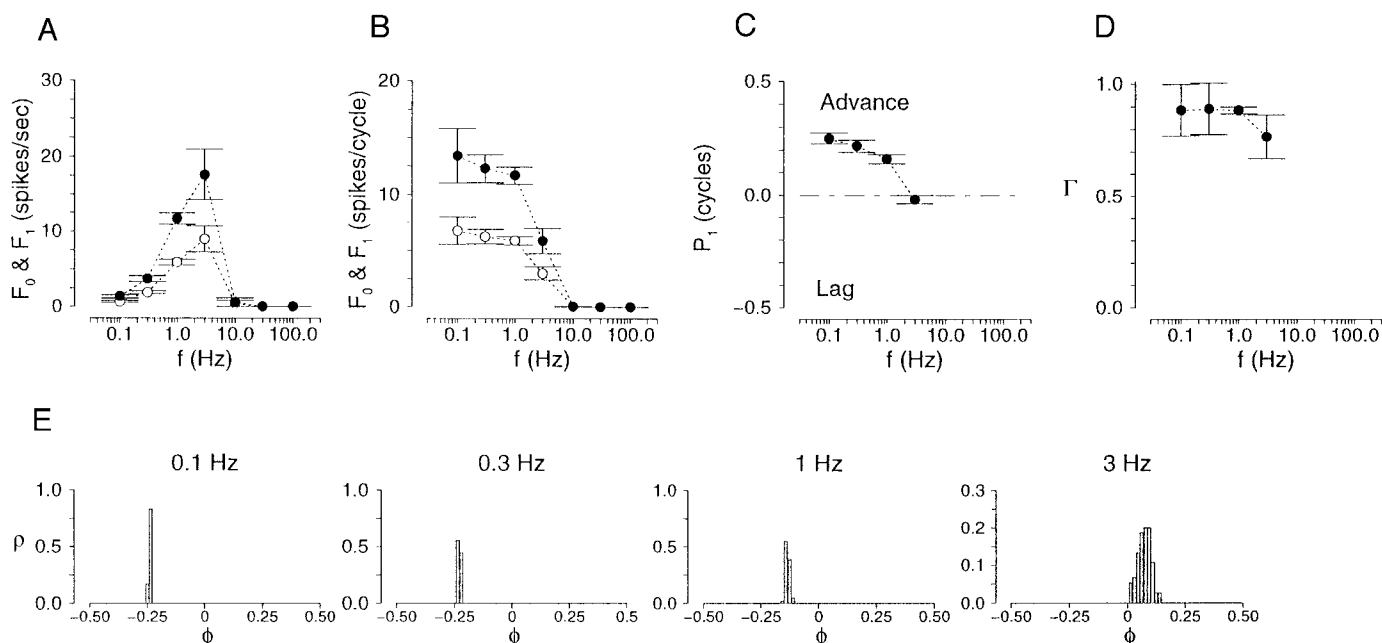
FIG. 8. Fourier analysis of relay neuron burst responses to sinusoidal current injection. *A–D*: data from 84 trials (8 different cells) in which only burst responses were observed. Mean ± SD (in pA): $I_0 = -56 \pm 112$, $I_1 = 191 \pm 14$. Circles and bars indicate the mean ± SE for response measures (F_0, F_1, P_1, and Γ) as a function frequency (f). Mean firing rate (F_0, open circles) and modulation-driven component of the response (F_1, filled circles) are plotted first in units of spikes/s (*A*) and subsequently in units of spikes/cycle (*B*). Also shown as a function of temporal frequency are the phase of the modulated response component (*C*) and index of nonlinearity (*D*). *E*: SPDHs for a single neuron responding in burst mode to applied current of different frequencies. This neuron did not respond at ≥10 Hz. Three-hertz response is 1 burst/cycle.

model tonic responses (Fig. 11) are also comparable with experimental records (Fig. 9), though a notable exception is a gradual drop in Γ at 30–100 Hz that is seen experimentally but not reproduced (cf. Figs. 9*D* and 11*D*). Again, this difference may reflect the presence of noise in the experimental recordings because we would expect a uniform amount of spike jitter (in units of time) to be more apparent in SPDHs obtained during high-frequency stimulation (when bins of phase correspond to shorter time intervals). Because in the in vivo experimental condition there is more synaptic (and other sources of) noise than encountered in vitro, we would expect less phase locking and more linearity in vivo than we have seen experimentally here (Carandini et al. 1996). Nonetheless, phase-locked relay neuron responses to drifting sinusoidal contrast gratings have been observed in vivo (Reich et al. 1997, 1998).

There is also a reasonable agreement between experiment and theory in analysis of tonic firing (Figs. 9 and 11), which, in turn, indicates that the IFB model exhibits most of the major differences between burst and tonic response modes actually seen in relay cells. The F_0 and F_1 response measures in the model (Fig. 11, *A* and *B*) closely follow experimental results. However, the relationship of response phase with stimulation frequency (Fig. 11*C*) is much flatter for lower frequencies than seen experimentally, and this difference is considered further in DISCUSSION. Also similar to experiment, the index of nonlinearity increases in the 0.1- to 3-Hz frequency range (Fig. 11*D*), but the model fails to show the decrease in nonlinearity with higher frequencies that is seen experimentally.

The SPDHs for the IFB model responding in tonic mode show a transition from superharmonic to subharmonic spiking that is qualitatively similar to that seen experimentally (cf. Figs. 9*E* and 11*E*). At low frequencies, the IFB model responds with superhar-

monic tonic spikes (many spikes/cycle). At 3 and 10 Hz, the model responds in a phase-locked fashion (4:1 and 1:1, respectively). At 30–100 Hz, phase-locked subharmonics responses are produced. Because of the strong phase-locking properties of the IFB model (Keener et al. 1981), the theoretical SPDHs in this frequency range are more focused than the experimental SPDHs. This causes Γ to be elevated compared with experiment in the 30- to 100-Hz range (cf. Figs. 9*D* and 11*D*).

Phase plane portrait of the IFB model and high-frequency roll off in burst mode

As the cutoff frequency is approached, burst responses of relay cells gradually decline or roll off (e.g., Fig. 8, *A* and *B*). One obvious reason for this is that some neurons exhibit subharmonic bursts in this frequency range, and this would cause a decrease in spikes/second and spikes/cycle. In a subset of trials that exhibited bursting in the range of 1–3 Hz, we found subharmonic (1:*N*) bursting and 1:1 bursting to be nearly equally prevalent at 3 Hz (36 and 43%, respectively), suggesting for some cells another reason for this roll off, one that is predicted by our IFB model. Figure 12*A* shows burst responses from the IFB model that demonstrate the roll off in F_0 during 1:1 bursting. At 2 Hz, the model responds with 1 burst/cycle, and each burst is composed of 6 spikes/burst. However, at 6 Hz, where 1 burst/cycle also is seen, only 2 spikes/burst are evoked. Also note that the maximum deinactivation levels (h_{max}) of I_T achieved during the hyperpolarizing phase of the applied current is much greater at 2 than 6 Hz (Fig. 12*B*). The greater h_{max} at 2 Hz thus leads to a larger evoked low-threshold Ca^{2+} spike, which, in turn, evokes more action potentials.

Figure 12*C* presents phase-plane portraits of the IFB model
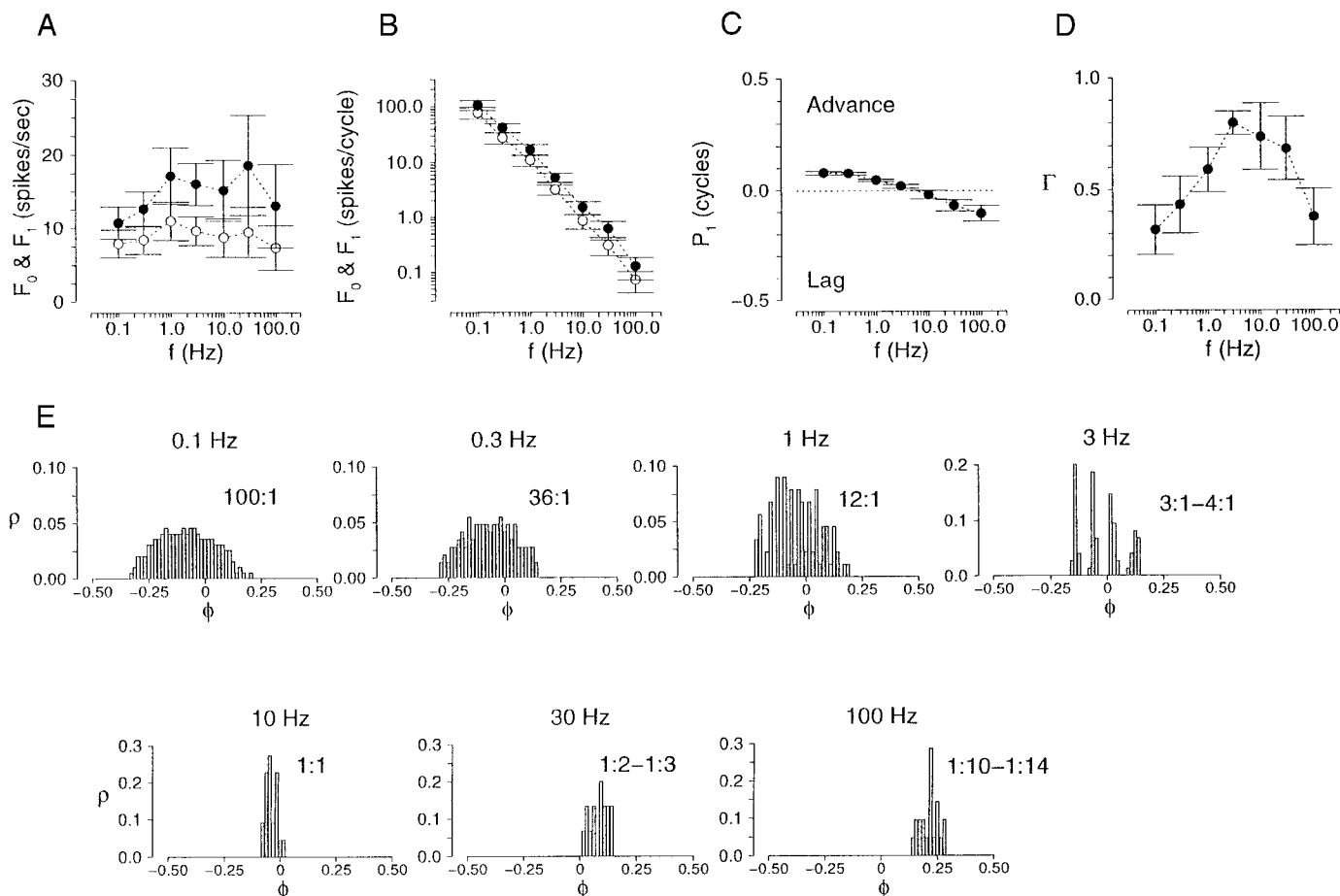
FIG. 9. Fourier analysis of relay neuron tonic responses to sinusoidal current injection. *A–D*: data from 88 trials (10 different cells) in which only tonic responses were observed. Mean ± SD (in pA): $I_0 = 465 \pm 133$, $I_1 = 193 \pm 13$. Conventions are identical to Fig. 9. F_0 and F_1 show no cutoff at high-frequency because I_0 was often superthreshold. *E*: SPDHs for a single neuron responding in tonic mode to applied current of different frequencies. Superharmonic and subharmonic responses (*S* spikes every *C* cycles) are indicated by *S:C*.

at 2 and 6 Hz. This helps to clarify the relationship between membrane potential (*V*) and thus spike discharge, and the inactivation gating variable, *h*, at both frequencies. The solid line and arrows show the trajectory in the (*V, h*) plane that is repeated from cycle to cycle. The threshold for I_T (V_h, dashed line), V_{reset} (dot-dashed line), and V_θ (dotted line) also are indicated. During the hyperpolarizing phase of the applied current, *V* eventually drops below V_h, causing *h* to increase (arrow 1). Eventually the current reverses, leading to depolarization; however, because *V* is still less than V_h, *h* continues to increase (arrow 2). When the membrane potential crosses V_h, I_T activates, *h* begins to drop, and I_T depolarizes the model neuron until the spike threshold, V_θ, is reached (arrow 3). A series of action potentials are evoked (arrow 4) and *h* decreases until the sum of I_T and the applied current are no longer large enough to bring the membrane potential above threshold. When the applied current again reverses, the membrane potential hyperpolarizes, *V* eventually drops below V_h, and the periodic burst response repeats.

Figure 12*D* shows a plot of the frequency-dependence of h_{max}. Because the time constant for inactivation of I_T is smaller than the time constant for its deinactivation (see METHODS), h_{max} decreases as frequency increases. This, in turn, means that the size of the evoked low-threshold Ca^{2+} spike and the number of

action potentials riding its crest will decrease at higher frequencies. It is thus this decline in h_{max} as a function of frequency that leads to the high-frequency roll off in the IFB model burst response. Although we do not have direct access the gating variable, *h*, in our experimental recordings, the open squares and diamonds in Fig. 12*E* show the number of spikes/burst exhibited by two relay neurons that burst 1:1 at all frequencies tested. This qualitatively matches roll off in spikes/burst exhibited by the IFB model (open circles) using standard parameters, although a better fit for these particular trials was obtained by increasing τ_h^+ from 100 to 300 ms, which resulted in a lower cutoff frequency (filled circles).

Dependence of response measures on modulation amplitude

In the analyses summarized in Figs. 8–11, I_1 was fixed and small enough to avoid burst followed by tonic responses, and I_0 controlled the response mode by being either relatively depolarizing (for tonic firing) or hyperpolarizing (for burst firing). However, in both modes, the quantitative value of response measures depends on I_0 and I_1. This is true for both actual relay cells as well as the IFB model. Figure 13, *A–C, left,* presents the frequency dependence of the fundamental response F_1 for 11 relay neurons using either low I_1 (50–200 pA;
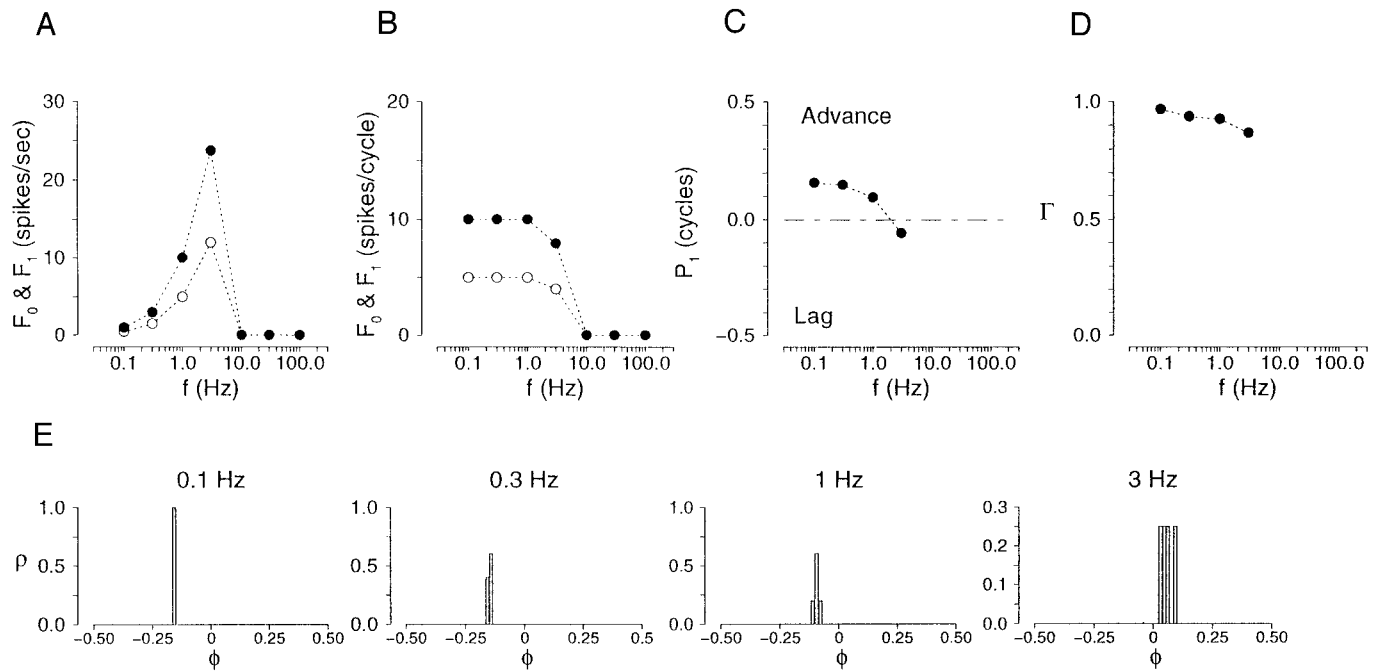
FIG. 10. *A–D*: Fourier analysis of IFB model burst responses to sinusoidal current injection (cf. Fig. 8). $I_0 = 0$ μA/cm^2 and $I_1 =$ 0.33 μA/cm^2. *E*: SPDHs for IFB model responding in burst mode to applied current of different frequencies.

filled squares) or high I_1 (300–500 pA; open triangles), and the *right panels* show the comparable responses from the IFB model. These results are pooled according to the firing mode based on I_0 so that Fig. 13*A* (I_0 *high*) presents responses that are predominantly tonic, whereas Fig. 13*C* (I_0 *low*) presents predominantly burst responses, and Fig. 13*B* (I_0 *medium*) includes many burst followed by tonic responses.

Note that the fundamental response is generally greater in Fig. 13 for the higher I_1 than for the lower regardless of response mode. During tonic firing (Fig. 13*A*), there is little if any frequency dependence in the response augmentation with higher I_1. However, when bursting occurs (Fig. 13, *B* and *C*) the degree of augmentation for large I_1 can be frequency dependent. For example, the experimental responses show a greater F_1 for the larger I_1 at lower frequencies, but there is little difference in F_1 at 10–100 Hz (note the overlapping error bars in Fig. 13*B*, *left*, for these frequencies). Qualitatively, this pattern is matched in the IFB model (Fig. 13*B*, *right*), which shows a clear peak in the augmentation of F_1 with I_1 at 3 Hz and no difference in response to higher frequencies. In experimental observations of burst mode (Fig. 13*C*, *left*), there is a clear distinction between low and high I_1.

Because with the fairly stable number of spikes/burst we observe, the response in spikes/seconds becomes increasingly small at lower frequencies. The IFB model qualitatively exhibits these same features (Fig. 13*C*, *right*), and the response function for F_1 reproduces this band-pass characteristic. However, for the most part this attenuation is "artificial," that is, it simply reflects the fact that the response is measured in spikes/second. To clarify this point, the solid squares in Fig. 13*D* redisplay in units of spikes/cycle F_1 for the low I_1 case shown previously (Fig. 13*C*, solid squares). In these units the neuronal response is low-pass rather than band-pass (cf. Fig. 8, *A* and *B*).

At the lowest values of I_1 tested, we found that 6 of 11 neurons were unresponsive to the lowest frequencies tested but

responsive to higher ones (see Fig. 5), while the remaining 5 responded to even the lowest frequencies. The open circles in Fig. 13*D* show the average F_1 in units of spike/cycle. The F_1 is attenuated at 0.1 Hz relative to the 0.3- and 3-Hz response, even when measured in units of spike/cycle (Fig. 13*D*, open circles). This occurs because approximately half of the trials were genuinely band-pass, that is, for this low value of I_1, 50% of the neurons did not respond at 0.1 Hz even though they did respond with 1 burst/cycle at 0.3 Hz.

Parameter studies of IFB model responses

To give a sense of the dynamics of transitions between tonic and burst modes of firing as parameters vary, Fig. 14, *A–C*, presents a series of raster plots calculated using the IFB model in which I_0 is varied while the frequency and cellular parameters are fixed, and amplitude of modulation increases from *A* to *C* (see legend of Fig. 14 for details). In Fig. 14*A*, where I_1 is low, as I_0 becomes more depolarizing, one sees a transition from silence to burst responses to another silent zone and then to tonic responses. Another transition in Fig. 14*A* is observed near $I_0 = 1.4$ μA/cm^2, where tonic spikes occur throughout the stimulus cycle (as opposed to the interrupted spiking). This happens when I_0 is sufficiently depolarizing to ensure that, when added to I_1, the model cell's membrane potential is always continuously driven above threshold for action potentials. The open circles in Fig. 14*A* show the phase of the centroid of the response (P_1) plotted relative to the time of an applied current maximum (vertical dot-dashed line). Burst responses are phase lagged when first recruited at low I_0 but then advance in phase as I_0 is increased. Tonic responses evoked as I_0 becomes more depolarizing consistently have a phase near zero.

By allowing a close look at spike timing as I_0 is varied, the raster plot of Fig. 14*A* complements the Fourier analysis presented previously. For example, the phase of individual tonic
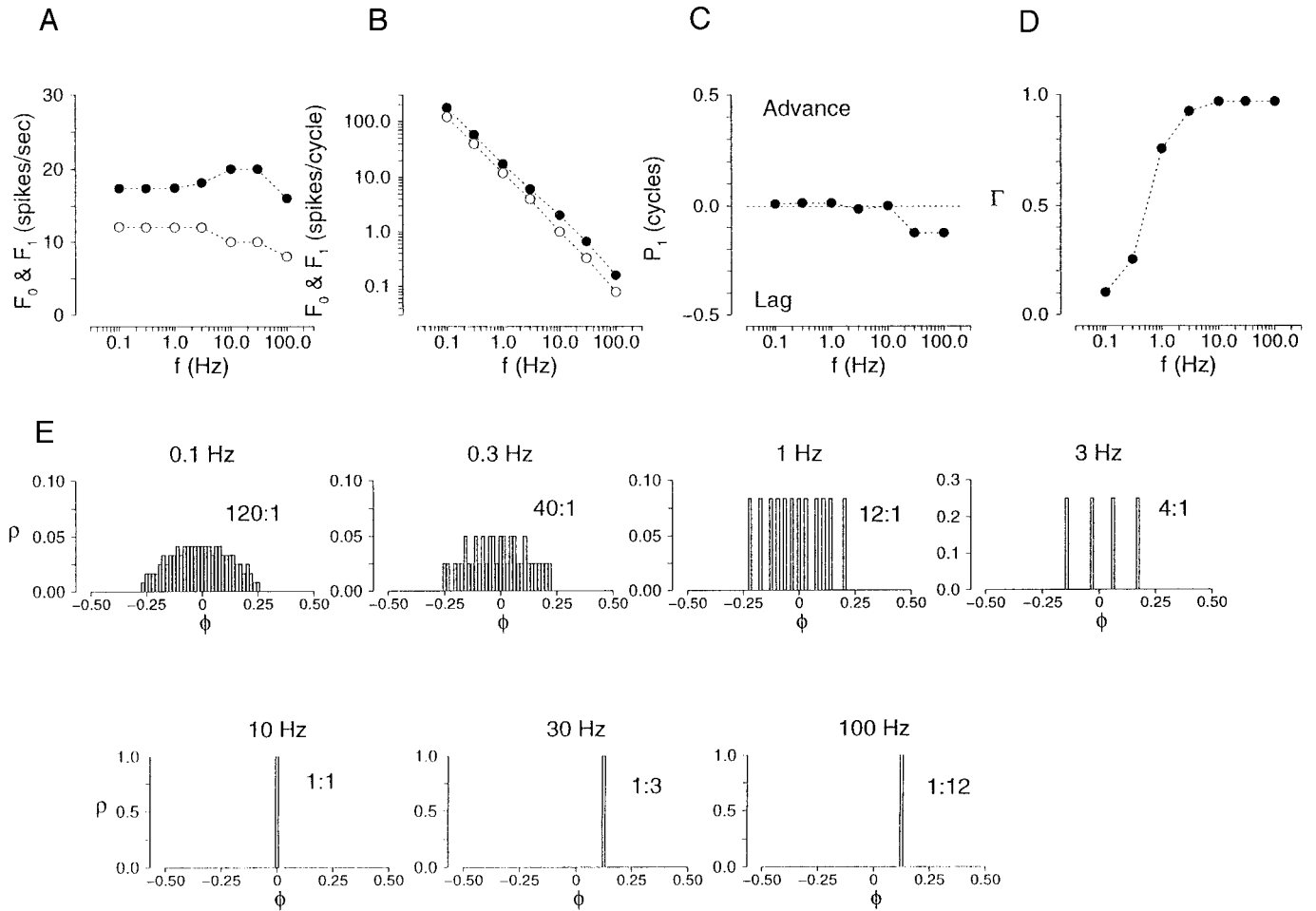
FIG. 11. *A–D*: Fourier analysis of IFB model tonic responses to sinusoidal current injection (cf. Fig. 9). $I_0 = 1.11$ $\mu A/cm^2$ and $I_1 = 0.67$ $\mu A/cm^2$. *E*: SPDHs for IFB model responding in tonic mode to applied current of different frequencies. Superharmonic and subharmonic responses (*S* spikes for every *C* cycles) are indicated by *S:C*.

spikes generally advances with increasing I_0. The new spikes that occasionally are recruited as I_0 increases generally appear in the late phase of the stimulus cycle, that is, when the applied current is decreasing. During interrupted tonic spiking, there is no consistent increase in P_1 as a function of I_0 because the gradual phase advance of individual spikes is balanced by new spikes arriving later in the cycle.

The gap between burst and tonic responses in Fig. 14*A* indicates a range of I_0 for which the IFB model does not respond. Such a gap also was observed experimentally (data not shown) and is present in the IFB model when I_1 is small enough so that, over a certain range of I_0, the membrane potential oscillates in response to the applied current without crossing either of the two thresholds, V_θ or V_h. This gap is reduced or nonexistent with larger values of I_1 (Fig. 14, *B* and *C*). Figure 14*B* shows the result of larger I_1, and here burst responses appear more robust, beginning at lower values of I_0 and extending into higher values. Comparing Fig. 14*A* and 14*B*, one also sees that increased I_1 extends the range of interrupted tonic firing to higher levels of I_0. In Fig. 14*C*, I_1 is made even larger, leading to burst followed by tonic responses over a large range of I_0. The transition point between interrupted and continuous tonic spiking has moved upward beyond $I_0 = 3.0$ $\mu A/cm^2$ and is no longer visible.

Figure 14, *D–F*, shows rastergrams of the IFB model burst responses as a function of the frequency of the applied current where the abscissa indicates the phase (ϕ) of each spike. Because of the compression of time in this coordinate at lower frequencies, the burst events appear to narrow, even though their duration is relatively constant. Figure 14, *D–F,* varies only in I_0, which is increasingly depolarizing from *D* to *F*. Figure 14*D* thus illustrates only burst responses, and comparing the open circles and vertical dot-dashed line here reveals that the phase advance of these responses gradually changes to a phase delay as the frequency increases from 0.1 to 10 Hz (cf. Fig. 10*C*).

In Fig. 14, *E* is similar to *D*, but I_0 is depolarizing, and interrupted tonic responses are evoked. Between 0.1 and 1 Hz, the fraction of the stimulus cycle occupied by tonic spikes is approximately constant. The IFB model here is responding relatively linearly (e.g., $\Gamma = 0.15$ at 0.3 Hz; see Fig. 11*D*). From 0.1 to 6 Hz, P_1 is approximately zero (cf. Fig. 11*C*) even though the phase of the first tonic spike advances considerably in the range of 1–6 Hz. Above 6 Hz, the model responds with 1 spike/cycle, and P_1 follows the phase lag of this solitary spike until the cutoff frequency is reached. Here the response in nonlinear (e.g., $\Gamma = 0.94$ at 10 Hz; see Fig. 11*D*). The low-pass character (no response at $\geq$30 Hz) of these tonic
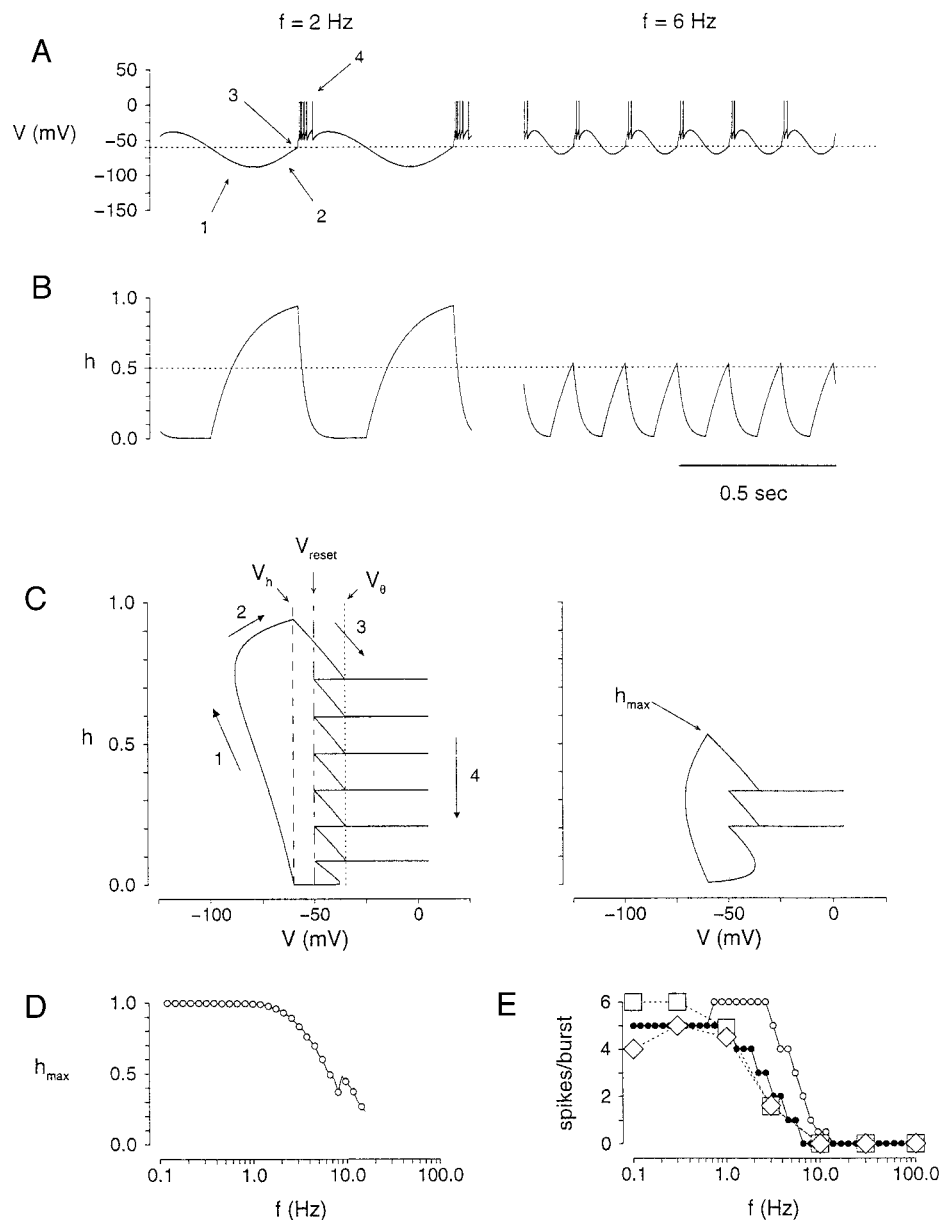
FIG. 12. Frequency dependence of I_T inactivation. *A*: membrane potential time course for IFB model at *f* of 2 (*left*) and 6 Hz (*right*). *B*: time course of *h*, the inactivation gate of I_T, at 2 and 6 Hz. *C*: *h* vs. *V* phase-plane portraits for the IFB model simulations shown in *A* and *B*. Dashed line (labeled V_h), threshold for deinactivation (and activation) of I_T; dot-dashed line (labeled V_{reset}), value to which the membrane potential is set after each spike; dotted line (labeled V_θ), action potential threshold. Arrows, direction of flow; numbers make correspondence between *C* and *A*. *D*: frequency-dependence of h_{max}, the maximum deinactivation level achieved during repetitive bursting. *E*: number of spikes/burst for both experimental observations and the IFB model. Shown are 2 representative relay neurons (open squares and diamonds), the IFB model with standard parameters (open circles), and the IFB model with $\tau_h^+ = 300$ ms (filled circles). I_0 and I_1 in μA/cm^2: 0.0, 1.0.

responses reflects the fact that I_0 is subthreshold for action potentials here. For comparison, Fig. 14*F* presents a calculation identical to *E* except that I_0 is increased to a level that is superthreshold. In this case, the IFB model responds with tonic spikes even at 100 Hz. Strong phase locking is seen at higher frequencies with low *S:C* ratios that change discontinuously with frequency.

The dual threshold character of the IFB model and the influence of I_0 on the functional dependence of F_0 and F_1 on I_1 is illustrated further in Fig. 15. With stimulation frequency fixed at 2 Hz, I_0 is more hyperpolarizing in the successive rows of Fig. 15, so that *A* exhibits purely tonic responses, *E* exhibits only burst responses, and *B–D* show gradual shift from pure tonic, to burst followed by tonic to pure burst responses. Voltage trajectories are presented for two representative values of I_1, the column labeled I_1 *Low* presenting simulations with a modulation amplitude that is small in comparison with the I_1 *High* column. These voltage trajectories are superimposed on

dotted and dashed lines, indicating the tonic spike threshold (V_θ) and I_T threshold (V_h), respectively.

In Fig. 15, the arrows labeled V_{ss} indicate the membrane potential that would be approached (in the absence of spiking) on the basis of the DC bias current alone so that $V_{ss} = V_L + I_0/g_L$, where V_L is resting membrane potential and g_L is leakage conductance of the model. Indeed, the relationship among V_{ss}, V_θ, and V_h determines the functional form of F_0 and F_1 as a function of I_1. For example, in Fig. 15*A*, I_0 is depolarizing enough that the steady-state voltage, V_{ss}, is greater than the threshold for action potentials ($V_{ss} > V_\theta$). Thus *low* I_1 gives continuous tonic spiking, whereas *high* I_1 gives interrupted tonic spiking. F_0 is thus nearly constant with I_1, whereas F_1 increases as a function of I_1. Compare this with Fig. 15*B*, where I_0 is less depolarizing, so that the steady-state voltage is near the action potential threshold ($V_{ss} = V_\theta$). In this case, *low* I_1 gives low-frequency interrupted tonic spiking, whereas *high* I_1 results in a burst followed by tonic response, because the
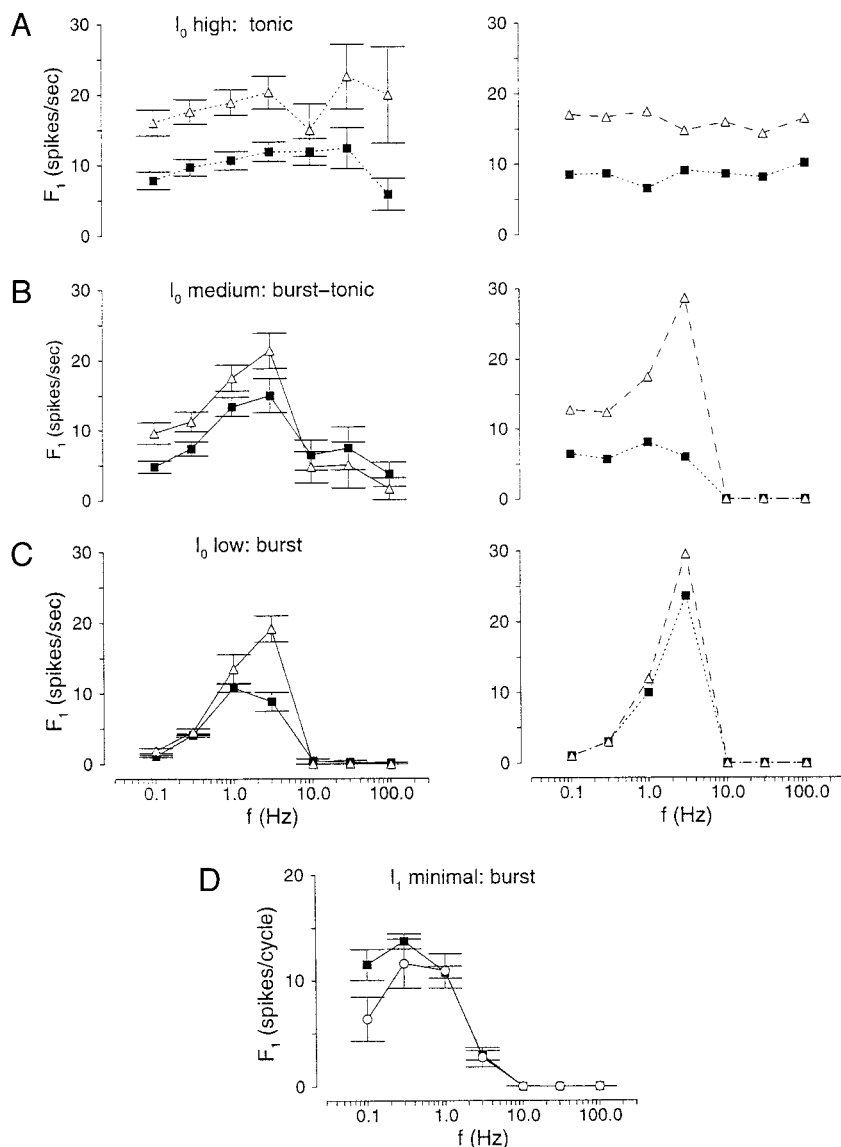
FIG. 13. *A–C*: fundamental responses, F_1, for relay neurons and IFB model over a range of I_0 and I_1. Response mode is controlled by I_0 so that the majority of the responses in *A* are tonic, the majority of the responses in *C* are burst, and *B* includes a large number of burst followed by tonic responses. Filled squares, I_1 is low; open triangles, I_1 is high. Error bars indicate mean $\pm$ SE. *D*: average response (F_1) per cycle as function of temporal frequency. Filled squares indicate data replotted from *C, left*. Open circles show a similar analysis when the lowest I_1 to which each cell responded was applied.

minimum membrane potential during a cycle is now less than V_h, thereby resulting in enough I_T deinactivation to allow the ensuing depolarizing half-cycle of the stimulus to evoke an early burst. Here F_1 is once again a nearly linear function of I_1; however, F_0 is no longer relatively constant as in Fig. 15*A* but rather has a similar slope as F_1. The voltage trajectory for the *low* I_1 case in Fig. 15*C* shows a null response followed after a threshold I_1 is exceeded by a fairly linear growth in both F_0 and F_1 with increasing I_1. Here V oscillates between V_θ and V_h for low values of I_1 (see Fig. 15*C, middle*) and, consequently, the IFB model does not respond for this particular value of I_0, resulting in a gap between burst and tonic responses visualized previously in the IFB model raster plot (Fig. 14*A*). In Fig. 15*D*, I_0 is such that that the steady-state voltage is near the burst threshold ($V_{ss} = V_h$, and a consequence of this is that even the lowest nonzero value of I_1 elicits a burst response. For Fig. 15*E*, the response is entirely composed of bursts, and F_0 and F_1 respond similarly with increasing I_1, showing a fairly sharp threshold when I_1 is sufficiently large to recruit bursts followed by a slight increase in firing.

The dependence of response measures on the value of

both the mean and modulated applied current is summarized in Fig. 16, which presents Fourier analysis of IFB model responses to 0.3-Hz stimulation over a range of I_0 and I_1 values. The front edge of the surface plot of F_0 in Fig. 16*A*, where I_1 is zero, is the current-frequency relation for the IFB model in tonic mode, that is, the classical leaky integrate-and-fire current-frequency relation (see APPENDIX). The rheobase occurs near 1.1 μA/cm^2, and, because we have not included an absolute refractory period in the spike generating mechanism of the IFB model, the current-frequency relation does not saturate and is approximately linear (except near the onset of repetitive firing), reaching 80 spikes/s at 4 μA/cm^2. When I_0 is hyperpolarizing, there is a value of I_1 above which the IFB model can respond. In the projection of the surface onto the horizontal plane, the leftmost region of nonzero response runs from near $I_0 = 0$ μA/cm^2 and $I_1 = 0$ μA/cm^2) to respective values of -4 and 3, reflecting the tradeoff between I_0 and I_1 that allows V, during the depolarizing phase of the applied current, to exceed V_h (see APPENDIX). These responses are due primarily to bursts, a fact reflected in the plots of P_1 and Γ (Fig. 16, *C* and *D*), which
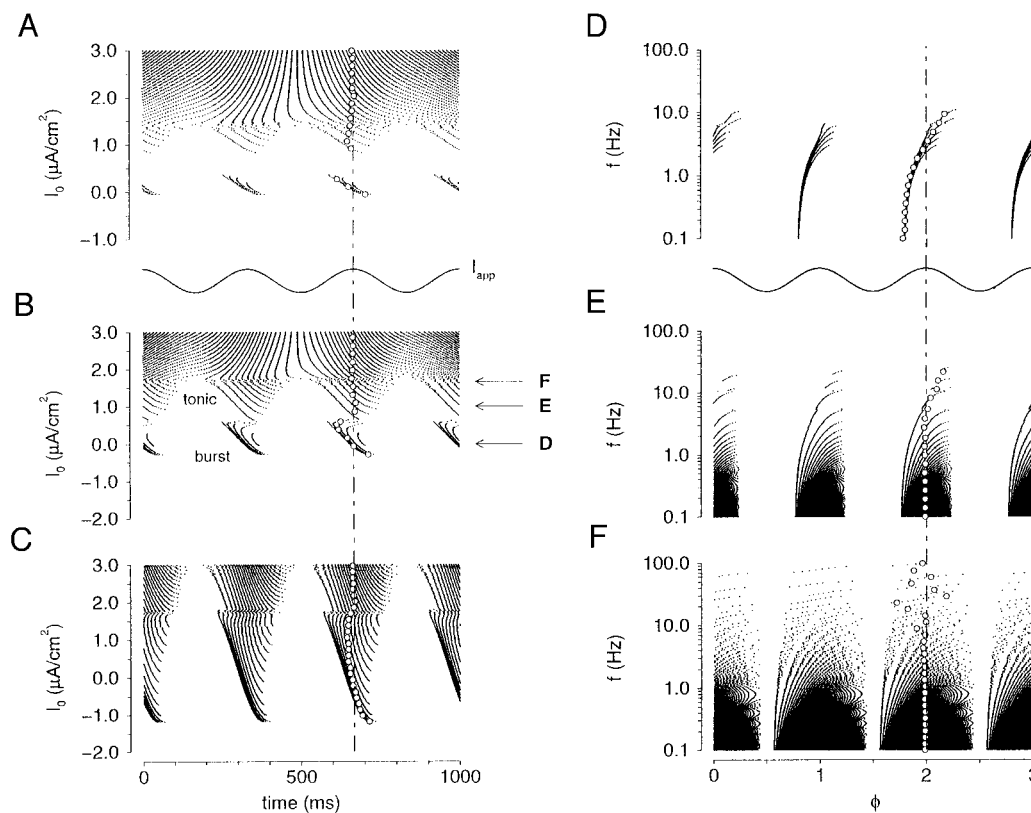
FIG. 14. Raster plots of IFB model responses to sinusoidal applied current. Each dot indicates the occurrence of a spike at a particular time or phase of the injected current. Raster plots are arranged vertically according to the value of a stimulus parameter (I_0 or f). Open circles, value of P_1; dot-dashed lines, phase 0. A–C: IFB model stimulated at 3 Hz and for a range of I_0. I_1 in $\mu A/cm^2$: A, 0.33; B, 0.67; C, 2.00. Labeled arrows, correspondence between parameter values and panels. Response is generally periodic at the stimulation frequency of 3 Hz. However, when I_0 induces continuous tonic spiking ($I_0 > 1.5$ in A and 1.75 in B), new dynamic phenomena arise—reminiscent of period doubling with the response repeating every few cycles. Also note that contrary to appearances, the firing frequencies during the 3 troughs in applied current occurring at $t = 166.67$, 500, and 833.33 ms are nearly identical. For example, inspection of the table of spike times for $I_0 = 3.0$ in B reveals a firing frequency at these troughs of 51.3, 51.0, and 51.3 Hz, respectively. Indeed, when all the points in the raster plot are removed save those associated with a single value of I_0, the 3 cycles are visually indistinguishable (except for a slight drift in phase). D: IFB model burst response over a range of frequencies. In $\mu A/cm^2$: $I_0 = 0.0$, $I_1 = 0.67$. E and F: IFB model tonic response when I_0 is subthreshold (1.0 $\mu A/cm^2$) or superthreshold (1.67 $\mu A/cm^2$), respectively. $I_1 = 0.67$ $\mu A/cm^2$.

show that the response near this interface is nonlinear and phase advanced. Figure 16B plots the dependence of F_1 on I_0 and I_1, which follows the same general trends as indicated in Fig. 16A, the one major exception being that F_1 is much less than F_0 when I_0 is high and I_1 is low (*bottom right* of graph). The largest discrepancies between F_0 and F_1 occur when the IFB model is tonic spiking in a modulated, but continuous, manner. In Fig. 16D, the peaks of elevated Γ that occur when $I_0 > 1.1$ $\mu A/cm^2$ and reflects phase locking that occurs when the firing frequency of the IFB model (determined solely by the DC current, I_0) are such that an integral number of spikes occur in one stimulus cycle. This phase locking is artifactual in the sense that when $I_1 = 0$ the stimulation frequency of 0.3 Hz is relevant only because it defines the Fourier fundamental frequency.

Figure 17 is identical to Fig. 16 except that the stimulus frequency is 3 Hz. One distinction between the low- and high-frequency results can be seen by comparing the surface plots for P_1 (Figs. 16C vs. 17C). In the 0.3-Hz case, the responses are always phase advanced. However, in the 3-Hz case, both phase advance and phase lag are observed depending on I_0 and I_1 (as in Fig. 14A). There is also a

significant region of the response surface in which Γ at 3 Hz is elevated compared with 0.3 Hz (Figs. 16D vs. 17D). This reflects phase locking that is more prominent at the higher frequency.

DISCUSSION

Our results provide further support for the functional differentiation between burst and tonic response modes in thalamic relay neurons. From intracellular recordings of relay neurons in the cat's lateral geniculate nucleus in a thalamic slice preparation, we have used Fourier analysis to quantify the response properties of relay neurons in different discharge modes. We concentrated on the temporal tuning of four relay cell response measures: F_0, F_1, P_1, and Γ. We found that the temporal tuning of relay neurons in cat is highly dependent on response mode (i.e., burst vs. tonic). Also these differences with respect to response mode were well captured using a relatively minimal IFB neuron model. Because the behavior of this simple neuronal model closely resembles our experimental data, it should prove useful for predicting population activity.
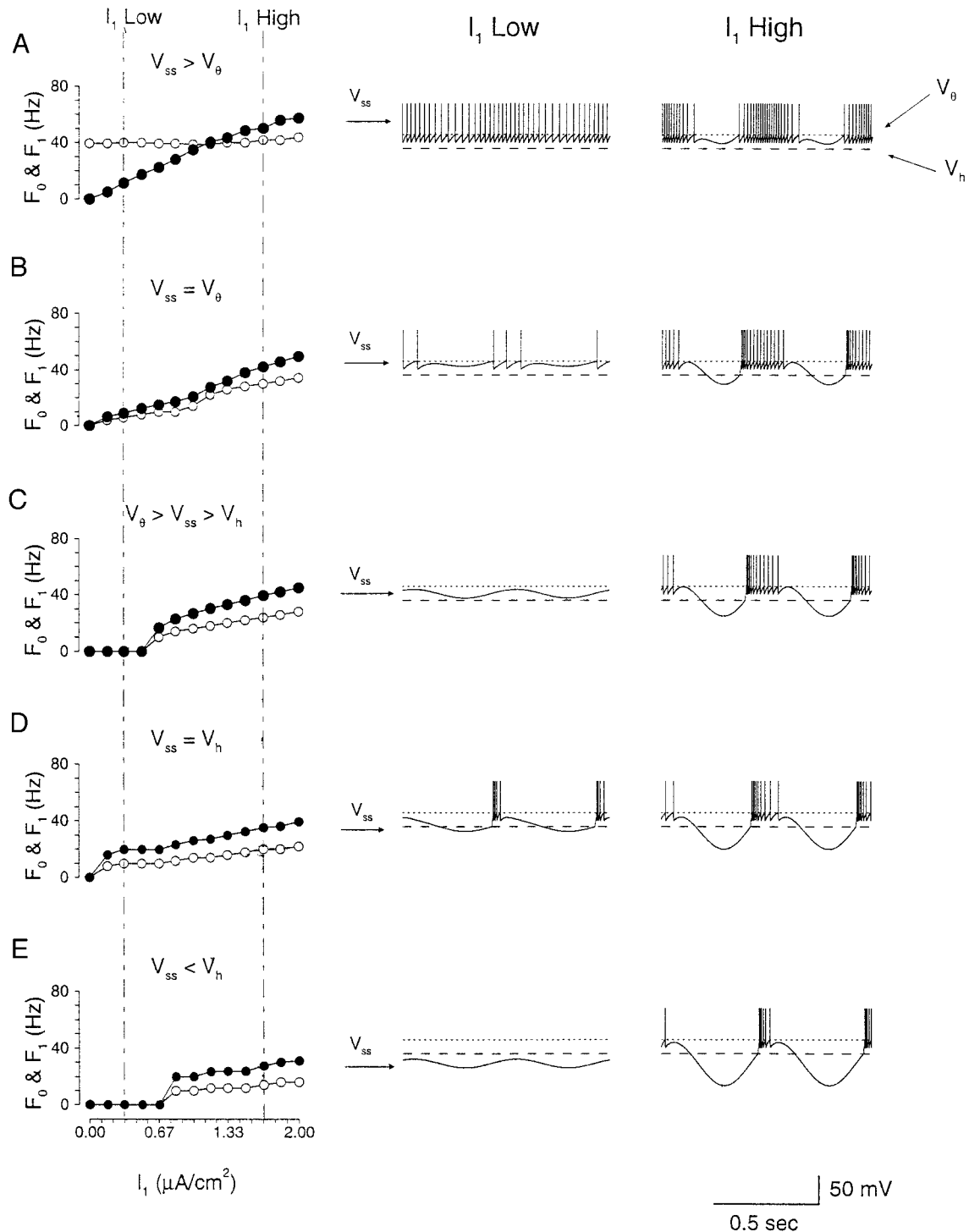
FIG. 15. *A–E, left*: F_0 (open circles) and F_1 (filled circles) as a function of I_1 for 2-Hz IFB model responses. I_0 is depolarizing in *A* and becomes hyperpolarizing in *E*. Arrows labeled V_{ss} indicate membrane potential that would be achieved due to the DC bias in the applied current (in the absence of spiking). *Middle* and *right* (labeled $I_{1\,low}$ and $I_{1\,high}$): voltage time courses for I_1 values of 0.33 and 1.67 $\mu A/cm^2$, respectively. Dotted lines, tonic spike threshold, V_θ; dashed lines, burst threshold, V_h. For *A–E*, respectively, I_0 in $\mu A/cm^2$: 2.0, 1.0, 0.58, 0.15, −0.43.

Responsiveness

The responsiveness of relay neurons to temporal frequency was markedly different between burst and tonic firing whether we measured the mean response (F_0) or the fundamental, modulated response component (F_1). In terms of temporal tuning, burst firing was low-pass for higher values of stimulus intensity (I_1) but markedly band-pass for lower values of I_1 (Figs. 5 and 8, *A* and *B*). In contrast to burst mode, the responses in tonic mode was broadband for the stimulus frequencies and intensity levels tested (see Figs. 5 and 9, *A* and *B*). Thus the tonic responses to very low frequencies were relatively robust. Our results for burst firing are consistent with
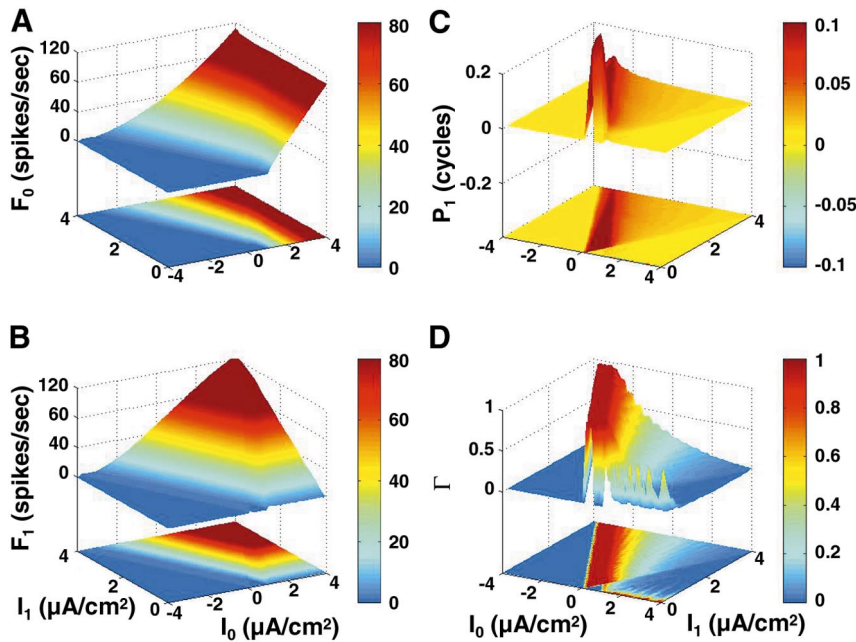
FIG. 16. Surface plots of response measures, F_0, F_1, P_1, and Γ, as a function of both I_0 (0–4 μA/cm²) and I_1 (−4–4 μA/cm²) for the IFB model stimulated at 0.3 Hz.

in vivo temporal tuning measurements derived from extracellular recordings in anesthetized cats (Mukherjee and Kaplan 1995), where retinogeniculate transmission during burst responses to visual stimulation were described having a temporal band-pass characteristic and during tonic firing were tuned more broadly. Also although responses in burst mode rarely were observed at 10 Hz regardless of I_1, neuronal responses in tonic mode routinely were observed at 30 and 100 Hz. This is qualitatively consistent with an in vitro study of guinea pig thalamic neurons (McCormick and Feeser 1990) that reported a high-frequency cutoff for repetitive burst responses near 10 Hz. The higher value obtained in this case may reflect the different stimuli used, i.e., square pulses versus sinusoids.

Another feature of the high-frequency cutoff in burst mode that we observed was the attenuation rather than an abrupt

cutoff of the F_0 and F_1 values at 3 Hz measured as spikes/cycle (see Fig. 8B). This could arise from two different properties that we observed in the experimental results. First, in about half the neurons, we observed subharmonic responses at 3 Hz and this would result in a decrease in spikes/cycle when averaged over a number of trials. Second, although individual bursts at lower frequencies (<3 Hz) evoked essentially the same number of action potentials, neurons that did not respond with subharmonic bursts at 3 Hz often exhibited response attenuation via a decrease in the number of spikes/burst (Fig. 12D). Although the IFB model is too idealized to account for subharmonic burst responses, it does reproduce this reduction of spikes at higher frequencies (Fig. 12D). Previous computational work also has indicated that, during repetitive hyperpolarizing current pulses, I_T gradually decreases at higher fre-
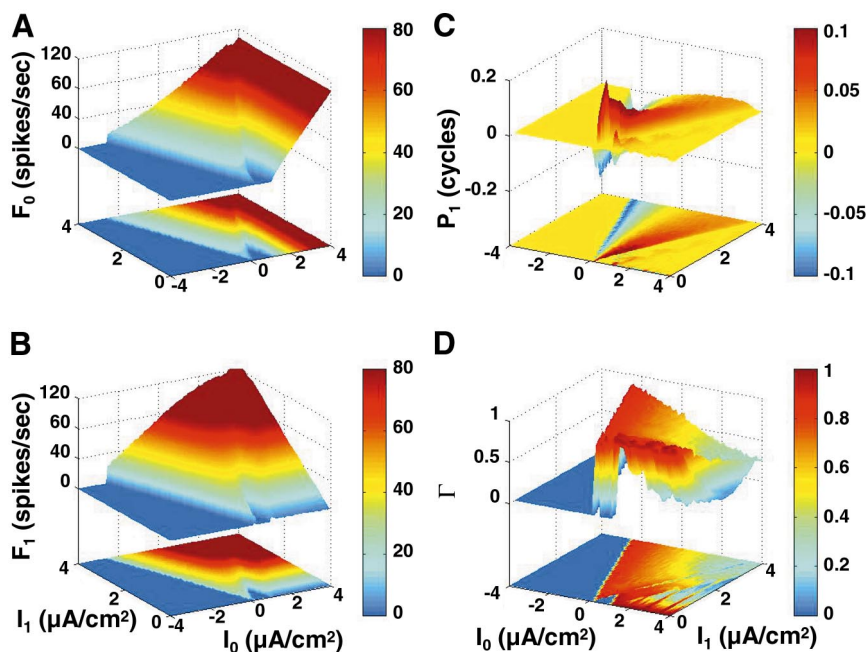

FIG. 17. Same as Fig. 16 except that the IFB model is stimulated at 3 Hz.

quencies (Wang et al. 1991) and thus likely would evoke fewer action potentials.

Burst firing in response to sinusoidal current injection thus is tuned to roughly 0.3–3 Hz, particularly for lower amplitudes of activation. The failure of burst responses to higher frequencies is due to the low-pass filter properties of the membrane that lead to attenuated voltage responses at high frequencies of injected current (this also applies to tonic responses) and to the time constant for deinactivation of I_T, which imposes a relative refractory period for the low-threshold Ca^{2+} spike, thereby limiting the high-frequency response. The IFB model responding in burst mode reproduces the high-frequency attenuation of F_0 and F_1 (Figs. 10, *A* and *B,* and 12*D*). However, it should be noted that this success is due in part to the fact that these response measures do not distinguish between subharmonic burst responses and reduction of spike/burst at higher frequencies.

The attenuation of burst responses observed at lower frequencies with moderate I_1 values is a result of a fairly constant number of action potentials per burst in conjunction with one burst per stimulus cycle. When the response is measured in spikes/second, this results in an apparent attenuation at lower frequencies. However, the lowest I_1 values giving rise to a burst response at 1–3 Hz resulted in no response at 0.1 or 0.3 Hz in 6 of 11 cells tested (see Fig. 5). The origin of the low-frequency cutoff observed in some relay neurons can be understood by considering models that are biophysically more detailed than the IFB model. Such models can be tuned to conform to our experimental observation that many relay neurons do not burst repetitively in response to any steady level of hyperpolarizing applied current. When this is done, one discovers that the membrane potential must exceed both a voltage threshold and also a minimum rate of change of the membrane voltage (i.e., dV/dt) to activate I_T. A limitation of the minimal IFB model is that it lacks this latter requirement, that is, the IFB model responds with a low-threshold spike no matter how slowly V is brought above the burst threshold, V_h.

Our experimental observation of band-pass relay neuron responses (in units of spike/cycle) may be of particular interest for the following reason. Fast EPSPs, such as those activated via ionotropic receptors (Conn and Pin 1997; Pin and Duvoisin 1995; Recasens and Vignes 1995), create a large enough dV/dt to activate I_T reliably. Much slower EPSPs, such as those activated via metabotropic receptors (Conn and Pin 1997; Pin and Duvoisin 1995; Recasens and Vignes 1995), might be so slow that the cell may depolarize without activating I_T. This also raises the possibility that EPSPs activated by metabotropic receptors could bring the cell from a hyperpolarized, burst-capable voltage regime to tonic firing mode by moving I_T from the deinactivated state to inactivated without ever activating I_T. If this metabotropic-based depolarization was strong enough, tonic firing would be evoked because there is no low-frequency attenuation for responses in tonic mode. We know that retinal inputs activate only ionotropic glutamate receptors on relay cells (Godwin et al. 1996; McCormick and von Krosigk 1992) and are thus likely to activate I_T reliably when the relay cell is in burst mode. Both cortical and brain stem modulatory inputs activate ionotropic and metabotropic receptors (Godwin et al. 1996; McCormick and von Krosigk

1992; reviewed in Sherman and Guillery 1996), which raises the intriguing possibility that activation of metabotropic receptors via these inputs can change the relay cell's firing mode without activating the cell.

Phase of response

During burst firing, both the experimental data and the IFB model show an overall phase advance that lags slightly with increasing temporal frequency (Figs. 8*B* and 10*B*). Because burst responses tend to be focused in phase, the quantitative value of P_1 is largely determined by the phase of burst onset. The phase advance exhibited by the IFB model at 0.1 Hz reflects the fact that V passes over the burst threshold, V_h, during the upswing of the sinusoidal current injection; however, the quantitative value ($P_1 = 0.2$ cycles) is sensitive to both I_1 and I_0 (e.g., the burst occurs earlier and is consequently more phase advanced with greater I_0). The decrease in phase advance with increasing frequency reflects the passive membrane properties in the subthreshold regime ($V < V_h$), that is, V can be delayed ≤90° with respect to the applied current when the IFB model is stimulated at higher frequencies (see *Eqs. A2* and *A3* in APPENDIX).

Tonic firing is different because there is less of a phase advance in the experimental data with a slight lag with increasing frequency and virtually no advance or change with frequency in the model. The reduced advance compared with burst firing can be explained by the fact that tonic firing provides a sustained response that will more symmetrically distribute around the peak of the sinusoidal stimulus. The subtle difference between the phase advance seen in tonic firing experimentally versus none in the model can be explained by the modest spike frequency adaptation (Vergara et al. 1998; Wang 1998) seen in geniculate relay cells (Smith et al. 1999). Spike frequency adaptation means that the response to a sustained input gradually reduces with time, and the result with a sinusoidal stimulus is that the responses will be slightly stronger before the peak of the sinusoidal stimulus than after. This, in turn, is reflected in a slight phase advance. Because the IFB model does not have spike frequency adaptation, it does not show this phase advance for tonic firing.

Linear summation of responses

The index of nonlinearity also differed greatly between the two firing modes, at least for low stimulus frequencies (0.1–1 Hz). Here tonic responses showed excellent linear summation, whereas burst firing did not, and this difference was captured effectively by the IFB model (Figs. 8*D*–11*D*). Our analysis indicates that this difference in linearity at lower temporal frequencies is largely due to the greater rectification of burst than of tonic responses. With increasing frequency of stimulation, the nonlinearity index during tonic mode became very similar to burst mode. However, here our analysis indicates that this increase in nonlinearity for tonic firing is a result not of increased rectification of the response but rather of phase locking of the response to the stimulus. This is curious because analogous measures of linearity of responses of geniculate cells to visual stimuli recorded in vivo indicate that tonic responses are reliably more linear than are burst responses at temporal frequencies that includes the range tested here (Guido et al.

1992, 1995; Mukherjee and Kaplan 1995). Our IFB model suggests an answer to this conundrum: when sufficient current noise is added to the neuron model, the phase locking seen for ≥ 3 Hz is largely eliminated, and tonic responses remain much more linear than burst responses. Similar effects have been observed in vivo during current injections of regular-spiking cells of the visual cortex (Carandini et al.1996) Because there is clearly more noise, such as synaptic noise, during in vivo recording than the sort of in vitro recording represented in Fig. 9*D*, we would expect a reduction in phase locking during tonic firing in vivo. However, it is interesting in this context to note that Reich et al. (1997) do find evidence for some phase-locking in responses to drifting sinusoidal gratings during in vivo recording in the cat lateral geniculate nucleus, but the phase locking was seen only to the highest contrast gratings used.

IFB model

An integral part of this work is the construction and tuning of a minimal model that quantitatively reproduces salient features of the thalamic relay cell firing patterns, including the burst/tonic differences discussed in the preceding text. The conceptual novelty of the IFB model is the compact account of both burst and tonic response properties of relay cells in terms of two thresholds, V_h and V_θ, responsible for the activation of burst and tonic spiking, respectively. When responding in tonic mode, the IFB model is essentially a classical leaky integrate-and-fire neuron model. When responding in burst mode, the dynamics of a single slow variable, h, characterize the inactivation and deinactivation of I_T that subserves burst firing. Unlike more complicated thalamic relay cell models, the IFB model is highly constrained to fit the Fourier analysis of experimental responses presented here.

It is remarkable that most of the Fourier analysis of experimental data is captured by the dual threshold character of the IFB model, and particularly so is the ability to quantitatively fit responses of cat geniculate relay cells with such a minimal characterization of I_T. Our observation that low-frequency injected current often fails to activate I_T even though higher-frequency stimulation is successful as well as the observation that many neurons do not repetitively burst for any range of injected current, together suggest a relatively small, if any, window current in these neurons (Coulter et al.1989). However, we have not explicitly probed for membrane potential bistability or other phenomenon that might be induced by a window current (Williams et al. 1997). Our success with the Fourier analysis using only a caricature of I_T is presumably due in part to the use of a (relatively simple) sinusoidal stimulus and our focus on neuronal responses at the (relatively coarse) level of PSTHs. Thus it will be important to explore the generalizability of the model by comparing experimental and theoretical responses to more complex stimuli. Similarly, although here we found it unnecessary to include in the IFB model the hyperpolarization-activated cation conductance, I_h, in other contexts this conductance is known to play a significant role (McCormick and Pape 1990a).

Although the IFB model reproduces subharmonic tonic responses of relay neurons, it does not reproduce the subharmonic bursts occasionally observed experimentally. An important question is what aspect of the simplicity of the IFB model is responsible for this limitation. When relay cells are responding with subharmonic bursts, often a perfunctory low-threshold spike occurs on the crest of the cycle directly preceding a robust burst. Thus the relay cell appears to accumulate deinactivation of I_T (i.e., h gradually increases) during missed cycles (i.e., those in which bursts responses do not occur). This suggests that the IFB model does not reproduce subharmonics in burst mode because the simplified kinetics of I_T used do not allow the gradual increase in h.

To test this idea, we looked for subharmonic responses in a mathematical model of the low-threshold spike that uses continuous activation and inactivation curves for I_T that are biophysically more realistic than the discontinuous curves used in the IFB model (Wang et al. 1991). In agreement with our experimental observations, we chose parameters for this model such that repetitive low-threshold spikes (superharmonics) were not expressed for any range of applied current. In a narrow frequency range, this low-threshold spike model exhibited subharmonic responses similar to those of the relay neurons presented here. In addition, in the low-threshold spike model, deinactivation *(h)* does indeed accumulate during missed cycles. Thus the inability of the IFB model to reproduce the subharmonic burst responses observed occasionally in experiments may be due to its minimal characterization of I_T. On the other hand, reproducing subharmonic burst responses with a mathematical model that lacks I_h does not eliminate the possibility that I_h contributes to the experimentally observed responses. Indeed, during periodic square pulse stimulation, relay neuron models that include both I_T and I_h can produce subharmonic bursts that appear to originate from the temporal integration of hyperpolarization by I_h (Wang 1994).

Conclusions

There are two broad conclusions we can draw from these studies. First, on the experimental side, we have used Fourier techniques to characterize the input/output properties of geniculate relay cells in tonic and burst firing mode. Among the findings was evidence that tonic firing showed low-pass and sometimes broadband temporal tuning, while burst firing was band-pass, peaking near 3 Hz and often not responding to stimuli administered at lower frequencies (e.g., 0.1 Hz). These data are consistent with in vivo observations based on receptive field properties (Mukherjee and Kaplan 1995) and suggest that burst firing is not very responsive to steady-state properties of the visual world but rather require temporal change. We also found that, for frequencies <3 Hz, tonic responses were more linear than burst responses, whereas phase-locking of tonic responses ≥ 3 Hz increased the nonlinearity of tonic responses to levels near those seen during burst firing. Studies of receptive field properties in vivo find, on the one hand, that tonic firing is generally more linear than is burst firing for geniculate cells (Guido et al. 1992, 1995; Mukherjee and Kaplan 1995) and, on the other hand, that phase locking can occur for very high contrast stimuli (Reich et al.1997). However, the relationships among phase locking, linearity, temporal frequency, and burst versus tonic firing mode in these in vivo studies has not been exhaustively explored. Nonetheless it seems clear that many of the receptive field properties noted above are at

least partly due to the membrane properties of the geniculate relay cells themselves, particularly with respect to I_T.

Second, on the theoretical side, we have been able to reproduce the salient features of relay neuron responses to sinusoidal input with a minimal IFB neuron model. The computational simplicity of this model makes it a good starting point for network simulations of retinogeniculate transmission that include important aspects of thalamic circuitry (e.g., GABAergic inhibition from local interneurons and neurons of the thalamic rectricular nucleus). One of the keys to understanding thalamic relay function will be to understand how thalamic circuitry and corticogeniculate feedback controls the burst and tonic firing modes of geniculate relay neurons.

APPENDIX

Current-frequency relation for the IFB model in tonic mode

When responding in tonic mode, the IFB model is essentially a classical leaky integrate-and-fire neuron model (Knight 1972). In the absence of bursting, h eventually decays to zero and, because it is inactivated, the low-threshold Ca^{2+} current, I_T, will not contribute to the dynamics of the membrane potential, V, which are effectively given by

$$C \frac{dV}{dt} = I_0 + I_1 \cos(2\pi f t) - g_L(V - V_L) \quad (A1)$$

This equation differs from *Eq. 3* presented in METHODS only because I_T has been set to zero and the applied (I_{app}) and leakage (I_L) currents have been made explicit. As before, the membrane potential, V, is reset whenever the membrane potential reaches the firing threshold, V_θ, such that $V(t) = V_\theta \Rightarrow V(t^+) = V_{reset}$.

Until V achieves the threshold for firing an action potential, V_θ, the membrane potential of the model neuron is given by *Eq. A1*, solutions of which take the form

$$V(t) = W(t) + [V(t_0) - W(t_0)] \exp[-(t - t_0)/\tau] \quad (A2)$$

where t and t_0 are the present and initial time, respectively, τ is the membrane time constant, given by $\tau = C/g_L$, and $W(t)$ is given by

$$W(t) = V_L + I_0/g_L + \frac{I_1/g_L}{1 + (2\pi f \tau)^2} [\cos(2\pi f t) + 2\pi f \tau \sin(2\pi f t)] \quad (A3)$$

The current-frequency relation for a classical leaky integrate-and-fire neuron model can be derived from *Eqs. A2* and *A3*. Setting $I_1 = 0$, the expression for $W(t)$ simplifies to $W(t) = V_L + I_0/g_L$, which is no longer a function of t. To calculate the interspike interval, T, for a given value of the DC-applied current, I_0, let $V(0) = V_{reset}$ and solve for the first value of T such that $V(T + t_0) = V_\theta$.

This gives

$$V_\theta = V_L + I_0/g_L + [V_{reset} - V_L - I_0/g_L] \exp[-T/\tau] \quad (A4)$$

which can be rearranged to give

$$T = \tau \ln \left[\frac{I_0/g_L + V_L - V_{reset}}{I_0/g_L + V_L - V_\theta} \right] \quad \text{for } I_0 > g_L(V_\theta - V_L) \quad (A5)$$

where the condition on this expression indicates that the applied DC current, I_0, has to greater than the rheobase of the neuron for tonic spiking to occur.

Estimates of cutoff frequency in tonic and burst mode

Until either the tonic or burst threshold is crossed, V will be given by *Eq. A2*. If neither threshold is crossed for sufficiently long time, V will be given by $V(t) = W(t)$ with $W(t)$ as in *Eq. A3*. This solution

represents the membrane potential oscillating under the influence of the sinusoidal applied current. Such responses were seen both experimentally and in simulations (Fig. 3, *A* and *B, bottom*). In the IFB model calculation in Fig. 3*B, left*, V is oscillating between the burst and tonic thresholds (i.e., in the gap region), whereas in Fig. 3*B, right*, V is oscillating below the burst threshold.

When the model is in the gap region, $V_h < V < V_\theta$. Because $V(t) = W(t)$ and $W(t)$ is dependent on frequency, it is possible to ask how much the frequency would have to be lowered in order for a tonic or a burst response to be evoked by the model. This certainly will not occur unless the maximum membrane potential exceeds V_θ (evoking a tonic spike) or the minimum membrane potential passes below V_h (required for a burst response). Focusing on the first possibility, we can find the maximum of $V(t) = W(t)$ by differentiating *Eq. A3* to give

$$W'(t) = \frac{I_1/g_L}{1 + (2\pi f \tau)^2} [-2\pi f \sin(2\pi f t) + (2\pi f)^2 \tau \cos(2\pi f t)] \quad (A6)$$

Solving for t_{max} that satisfies $W'(t_{max}) = 0$ we find

$$t_{max} = \frac{1}{2\pi f} \arctan(2\pi f \tau) \quad (A7)$$

where $0 < 2\pi f \tau < \infty$ and $0 < \arctan(2\pi f \tau) < \pi/2$. It can be shown that $W''(t_{max}) < 0$ confirming that this is a maximum. Substituting t_{max} into *Eq. A3* we find that

$$V_{max}(f, I_0, I_1) = V_L + I_0/g_L + I_1 G(f)/g_L \quad (A8)$$

where

$$G(f) = \frac{1}{1 + (2\pi f \tau)^2} [\cos(\arctan[2\pi f \tau]) + 2\pi f \tau \sin(\arctan[2\pi f \tau])] \quad (A9)$$

and *Eq. A8* has been written to emphasize that V_{max} is dependent on stimulus parameters as well as cellular parameters. In particular, note that $G(f)$ is a monotonically decreasing function of the stimulus frequency, f. Thus we can imagine lowering the stimulus frequency (thereby increasing V_{max}) until V_{max} achieves the tonic firing threshold, V_θ, which results in an implicit expression that gives an estimate of the cutoff frequency, f_{cutoff}

$$\frac{V_\theta - V_L - I_0/g_L}{I_1/g_L} = G(f_{cutoff}) \quad (A10)$$

where the numerator of the left-hand side of the equality is positive (by our assumption that the membrane potential was originally oscillating between the burst and tonic threshold), and f_{cutoff} is only defined if $G(0) > (V_\theta - V_L - I_0/g_L)/(I_1/g_L)$. From *Eq. A10* one can see that f_{cutoff} is a function of stimulus parameters (I_0 and I_1) as well as cellular parameters; consequently, the experimentally observed values of f_{cutoff} should not be taken to reflect an intrinsic limit on a relay neuron's firing frequency (e.g., the cutoff frequency in tonic mode for the neuron presented in Fig. 3*A* is only 3 Hz). Because $G(f_{cutoff})$ is a monotonically decreasing function, *Eq. A10* implies that increasing I_1 results in increasing the cutoff frequency in tonic mode. Also note that the cutoff frequency is dependent on the DC-appied current, I_0.

As a final point, notice that if we know the stimulus frequency, f, we can solve for the values of I_0 and I_1 necessary to elicit a bursts response. We arrive at an expression similar to *Eq. A10*

$$\frac{V_h - V_L - I_0^{cutoff}/g_L}{I_1^{cutoff}/g_L} = G(f) \quad (A11)$$

that can be rearranged in the following manner

$$I_1^{\text{cutoff}} = -\frac{I_0^{\text{cutoff}}}{G(f)} + \frac{g_{\text{L}}(V_h - V_{\text{L}})}{G(f)} \qquad (A12)$$

This expression shows the tradeoff between I_0^{cutoff} and I_1^{cutoff} that can occur while still allowing V to achieve the threshold for firing a burst, V_h. The line defined by this expression is negatively sloped and corresponds to the leftmost region of nonzero response that runs from near $I_0 = 0$ μA/cm^2 and $I_1 = 0$ μA/cm^2) to respective values of -4 and 3 (see plot of Γ and P_1 in Fig. 16, C and D).

REFERENCES

BLOOMFIELD, S., HAMOS, J., AND SHERMAN, S. Passive cable properties and morphological correlates of neurones in the lateral geniculate nucleus of the cat. *J. Physiol. (Lond.)* 383: 653–692, 1987.

CARANDINI, M., MECHLER, F., LEONARD, C., AND MOVSHON, J. Spike train encoding by regular-spiking cells of the visual cortex. *J. Neurophysiol.* 76: 3425–3441, 1996.

CONN, P. J. AND PIN, J. P. Pharmacology and functions of metabotropic glutamate receptors. *Annu. Rev. Pharmacol. Toxicol.* 37: 205–237, 1997.

COULTER, D., HUGUENARD, J., AND PRINCE, D. Calcium currents in rat thalamocortical relay neurons: kinetic properties of the transient, low-threshold current. *J. Physiol. (Lond.)* 414: 587–604, 1989.

GODWIN, D. W., VAN HORN, S. C., ERIIR, A., SESMA, M., ROMANO, C., AND SHERMAN, S. M. Ultrastructural localization suggests that retinal and cortical inputs access different metabotropic glutamate receptors in the lateral geniculate nucleus. *J. Neurosci.* 16: 8181–8192, 1996.

GUIDO, W., LU, S. M., AND SHERMAN, S. M. Relative contributions of burst and tonic responses to the receptive field properties of lateral geniculate neurons in the cat. *J. Neurophysiol.* 68: 2199–2211, 1992.

GUIDO, W., LU, S.-M., VAUGHAN, J., GODWIN, D., AND SHERMAN, S. Receiver operating characteristic (ROC) analysis of neurons in the cat's lateral geniculate nucleus during tonic and burst response mode. *Vis. Neurosci.* 12: 723–741, 1995.

HUGUENARD, J. AND MCCORMICK, D. Simulation of the currents involved in rhythmic oscillations in thalamic relay neurons. *J. Neurophysiol.* 68: 1373–1383, 1992.

JAHNSEN, H. AND LLINAS, R. Electrophysiological properties of guinea-pig thalamic neurones: an in vitro study. *J. Physiol. (Lond.)* 349: 205–226, 1984a.

JAHNSEN, H. AND LLINAS, R. Ionic basis for the electroresponsiveness and oscillatory properties of guinea-pig thalamic neurones in vitro. *J. Physiol. (Lond.)* 349: 227–247, 1984b.

KEENER, J., HOPPENSTEADT, F., AND RINZEL, J. Integrate-and-fire models of nerve membrane response to oscillatory input. *SIAM J. Appl. Math.* 41: 503–517, 1981.

KIM, U., BAL, T., AND MCCORMICK, D. Spindle waves are propagating synchronized oscillations in the ferret LGNd in vitro. *J. Neurophysiol.* 74: 1301–1323, 1995.

KNIGHT, B. W. Dynamics of encoding in a population of neurons. *J. Gen. Physiol.* 59: 734–766, 1972.

MCCORMICK, D. AND FEESER, H. Functional implications of burst firing and single spike activity in lateral geniculate relay neurons. *Neuroscience* 39: 103–113, 1990.

MCCORMICK, D. AND HUGUENARD, J. A model of the electrophysiological properties of thalamocortical relay neurons. *J. Neurophysiol.* 68: 1384–1400, 1992.

MCCORMICK, D. A. AND PAPE, H. C. Properties of a hyperpolarization-activated cation current and its role in rhythmic oscillation in thalamic relay neurones. *J. Physiol. (Lond.)* 431: 291–318, 1990a.

MCCORMICK, D. A. AND PAPE, H. C. Noradrenergic and serotonergic modulation of a hyperpolarization-activated cation current in thalamic relay neurones. *J. Physiol. (Lond.)* 431: 319–342, 1990b.

MCCORMICK, D. A. AND VON KROSIGK, M. Corticothalamic activation modulates thalamic firing through glutamate "metabotropic" receptors. *Proc. Natl. Acad. Sci. USA* 89: 2774–2778, 1992.

MUKHERJEE, P. AND KAPLAN, E. Dynamics of neurons in the cat lateral geniculate nucleus: in vivo electrophysiology and computational modeling. *J. Neurophysiol.* 74: 1222–1243, 1995.

PIN, J. P. AND DUVOISIN, R. The metabotropic glutamate receptors: structure and functions. *Neuropharmacology* 34: 1–26, 1995.

PRESS, W., TEUKOLSKY, S., VETTERLING, W., AND FLANNERY, B. *Numerical Recipes in C: The Art of Scientific Programming* (2nd ed.). Cambridge: Cambridge Univ. Press, 1992.

RECASENS, M. AND VIGNES, M. Excitatory amino acid metabotropic receptor subtypes and calcium regulation. *Ann. NY Acad. Sci.* 757: 418–429, 1995.

REICH, D. S., VICTOR, J. D., AND KNIGHT, B. W. The power ratio and the interval map: spiking models and extracellular recordings. *J. Neurosci.* 18: 10090–10104, 1998.

REICH, D. S., VICTOR, J. D., KNIGHT, B. W., OZAKI, T., AND KAPLAN, E. Response variability and timing precision of neuronal spike trains in vivo. *J. Neurophysiol.* 77: 2836–2841, 1997.

RINZEL, J. Models in neurobiology. In: *Nonlinear Phenomena in Physics and Biology*, edited by R. H. Enns, B. L. Jones, R. M. Miura, and S. S. Rangnekar. Alberta, Canada: Nato Advanced Study Institute, 1980, vol. 75, p. 347–367.

SHAPLEY, R. AND LENNIE, P. Spatial frequency analysis in the visual system. *Annu. Rev. Neurosci.* 8: 547–583, 1985.

SHERMAN, S. Dual response modes in lateral geniculate neurons: mechanisms and functions. *Vis. Neurosci.* 13: 205–213, 1996.

SHERMAN, S. AND GUILLERY, R. The functional organization of thalamocortical relays. *J. Neurophysiol.* 76: 1367–1395, 1996.

SHERMAN, S. AND GUILLERY, R. On the actions that one nerve cell can have on another: distinguishing "drivers" from "modulators." *Proc. Nat. Acad. Sci. USA* 95: 7121–7126, 1998.

SMITH, G., COX, C., SHERMAN, S., AND RINZEL, J. Spike-frequency adaptation in sinusoidally driven thalamocortical relay neurons. *Soc. Neurosci. Abstr.* 1427, 1999.

VERGARA, C., LATORRE, R., MARRION, N. V., AND ADELMAN, J. P. Calcium-activated potassium channels. *Curr. Opin. Neurobiol.* 8: 321–329, 1998.

WANG, X. J. Multiple dynamical modes of thalamic relay neurons: rhythmic bursting and intermittent phase-locking. *Neuroscience* 59: 21–31, 1994.

WANG, X. J. Calcium coding and adaptive temporal computation in cortical pyramidal neurons. *J. Neurophysiol.* 79: 1549–1566, 1998.

WANG, X.-J., GOLOMB, D., AND RINZEL, J. Emergent spindle oscillations and intermittent burst firing in a thalamic model: specific neuronal mechanisms. *Proc. Nat. Acad. Sci. USA* 92: 5577–5581, 1995.

WANG, X.-J., RINZEL, J., AND ROGAWSKI, M. A model of the T-type calcium current and the low-threshold spike in thalamic neurons. *J. Neurophysiol.* 66: 839–850, 1991.

WILLIAMS, S. R., TOTH, T. I., TURNER, J. P., HUGHES, S. W., AND CRUNELLI, V. The "window" component of the low threshold Ca^{2+} current produces input signal amplification and bistability in cat and rat thalamocortical neurones. *J. Physiol. (Lond.)* 505: 689–705, 1997.